CANCER

Mitigating T cell DNA damage during PARP inhibitor treatment enhances antitumor efficacy

Jiahao Liu[1,2]†, Xiaofei Jiao[1,2]†, Wei Mu[3]†, Huayi Li[1,2], Yu Xia[1,2], Yijie Wu[1,2], Li Zhu[3], Qing Zhong[1,2], Wen Pan[1,2], Xingzhe Liu[1,2], Minghua Xiang[1,2], Jiali Cheng[3], Haolong Lin[3], Xuejiao Zhao[1,2,4,5], Zhiyong Ding[6], Guang Hu[7], Gordon B. Mills[4,5], Ding Ma[1,2], Qinglei Gao[1,2]*, Yong Fang[1,2]*

Poly(ADP-ribose) polymerase inhibitors (PARPis) are a class of agents targeting DNA damage repair that have become standard therapy for epithelial ovarian cancer (EOC) and multiple other solid tumors. In addition to targeting DNA damage repair, PARPis actively modulate antitumor immune responses, with efficacy being partially dependent on T cell activity. Here, we found that patient T cells sustain DNA damage during PARPi treatment, which reduces treatment efficacy. Leveraging paired pre- and posttreatment tumor samples from a clinical trial of patients with EOC treated with neoadjuvant niraparib as monotherapy, we showed that the PARPi caused DNA damage, slowed proliferation, and increased apoptosis in T cells, which we validated both in vitro and in mouse models. A genome-wide CRISPR (clustered regularly interspaced short palindromic repeats) knockout screen in primary human T cells identified PARP1 as the principal mediator of PARPi-induced T cell death. T cell–specific deletion of *PARP1* or mutating *Parp1* at its binding sites in transgenic mice led to reduced T cell DNA damage during PARPi treatment, resulting in improved efficacy of PARPis, alone or in combination with immune checkpoint inhibition. We then engineered PARPi-tolerant CAR T cells using cytosine base editing, which decreased PARPi-induced PARP1 trapping and led to reduced PARPi-induced DNA damage, resulting in superior antitumor efficacy in xenograft models compared with parental CAR T cells. This study highlights the relevance of PARPi-induced DNA damage to T cells and suggests opportunities to improve the efficacy of PARPis as monotherapy or in combination with immunotherapy.

INTRODUCTION

Homologous recombination deficiency (HRD) is a hallmark of cancer, and poly(ADP-ribose) polymerase inhibitors (PARPis) exploit this genetic characteristic to induce DNA double-stranded breaks in cancer cells (*1*). Now, seven orally administered PARPis have received global approval for the treatment of ovarian, breast, prostate, and pancreatic cancers, with others under development (*2*). PARPis have already revolutionized the treatment for epithelial ovarian cancer (EOC), the most lethal gynecologic malignancy (*3*). Patients with EOC are often diagnosed at an advanced stage and present with widespread disease in the peritoneal cavity; heavy tumor burden at presentation leads to extensive minimal residual disease even after debulking surgery and postoperative chemotherapy (*4*). Because the development of precision treatments for EOC has lagged behind other cancers, PARPis are a notable exception that offer manageable tolerability, sustained tumor suppression, extended progression-free survival (PFS), and improved overall survival as maintenance therapies in both frontline (*5*, *6*) and recurrent settings (*7*, *8*). However, PARPis often result in incomplete tumor elimination, ultimately leading to treatment failure (*9*). There are also reports suggesting that the application of PARPis may induce disorders in myeloid cells (*10*, *11*).

PARPis have also been shown to enhance T cell–mediated antitumor immune responses (*12*), which may create an opportunity to continuously eliminate residual cancer cells. Previous studies have demonstrated that PARPis increase lymphocyte infiltration in tumor islets and reverse the immunosuppressive tumor microenvironment (TME) in EOC, correlating with prolonged survival (*13*, *14*). PARPis result in substantial DNA damage and cytosolic double-stranded DNA (dsDNA) accumulations in both *BRCA*-deficient and *BRCA* wild-type tumor cells, which activate the cyclic GMP–AMP synthase–stimulator of interferon genes (cGAS-STING) signaling pathway and initiate the type I interferon response, thereby enhancing T cell infiltration and activation (*15*). In addition, DNA damage caused by PARPis leads to the generation of neoantigens that can promote T cell recognition, activation, and cytotoxicity (*13*). PARPis also counteract immunosuppressive cells including myeloid-derived suppressor cells (*16*) and regulatory T cells within the TME (*14*, *17*). Despite that, the direct effects of PARPis on T cells remain poorly understood.

The combination therapies of PARPis and immunotherapies including immune checkpoint inhibitors (ICIs) and chimeric antigen receptor T (CAR T) cell therapy have been explored previously based on the observation that PARPis could invigorate antitumor immunity (*18*). ICIs block the interaction between immunosuppressive molecules like programmed cell death 1 (PD-1) or programmed cell death ligand 1 and T cells to reduce T cell exhaustion (*19*). However, ICIs have not achieved durable clinical responses in most of the patients with EOC, especially those with insufficient tumor-infiltrating lymphocytes. Although PARPis could theoretically potentiate ICI responses by recruiting T cells, combining PARPis and ICIs did not

[1]Department of Gynecological Oncology, Tongji Hospital, Tongji Medical College, Huazhong University of Science and Technology, Wuhan, 430030, China. [2]National Clinical Research Center for Obstetrics and Gynecology, Cancer Biology Research Center (Key Laboratory of the Ministry of Education), Tongji Hospital, Tongji Medical College, Huazhong University of Science and Technology, Wuhan, 430030, China. [3]Department of Hematology, Tongji Hospital, Tongji Medical College, Huazhong University of Science and Technology, Wuhan, 430030, China. [4]Division of Oncological Sciences, Oregon Heath and Sciences University, Portland, OR 97201, USA. [5]Knight Cancer Institute, Portland, OR 97201, USA. [6]Mills Institute for Personalized Cancer Care, Fynn Biotechnologies Ltd., Jinan, 250101, China. [7]Nanjing IASO Biotherapeutics Ltd., Nanjing, 210043, China.
*Corresponding author. Email: qlgao@tjh.tjmu.edu.cn (Q.G.); tongjify@tjh.tjmu.edu.cn (Y.F.)
†These authors contributed equally to this work.

improve antitumor efficacy in most clinical trials (*20*–*22*), and the underlying reasons remain unclear (*23*). Incorporating PARPis with CAR T cell therapy has the potential to address the immunosuppressive TME and inadequate CAR T cell infiltration into the tumor, potentially leading to active monitoring and continuous eradication of minimal residential disease (*24*). However, realizing this curative potential relies on effective CAR T cell expansion and persistence during PARPi treatment, which remains poorly explored.

Our finely annotated single-cell dissection of paired pre- and posttreatment samples from the phase 2 clinical trial of patients with EOC treated with neoadjuvant niraparib monotherapy (*14*) may offer insights into these knowledge gaps. Here, we identified elevated DNA damage in T cells after niraparib treatment and revealed its association with clinical responses and PFS. Using in vitro studies and mouse models, we further showed that mitigating PARPi-induced DNA damage within T cells holds critical importance for maximizing the benefits of PARPis as monotherapy or in combination with anti–PD-1 treatment or CAR T cell therapy.

RESULTS

Increased DNA damage is found in tumor-infiltrating T cells after neoadjuvant treatment with niraparib

Newly diagnosed, treatment-naive patients with EOC with unresectable disease received niraparib as neoadjuvant therapy in a prospective clinical trial named "Effectiveness and safety of niraparib as neoadjuvant therapy in advanced ovarian cancer with homologous recombination deficiency (NANT)" (NCT04507841). Single-cell RNA sequencing (scRNA-seq) data from 24 paired tumor samples from 12 patients, collected before and after neoadjuvant PARPi treatment, were processed (*14*) and used for analysis. Changes in $CD8^+$ and $CD4^+$ T cells were assessed, showing a reduction in the percentage of proliferative $CD8^+$ and $CD4^+$ T cell subtypes after niraparib treatment (in 11 of 12 patients) (Fig. 1, A and B). Furthermore, in T cells and $CD8^+$ T cells, we observed an elevated enrichment score for tumor protein 53 (TP53)–targeted apoptosis and DNA damage checkpoint pathways, along with a reduction of T cell proliferation, in posttreatment samples (Fig. 1, C and D).

Analysis of multiplex immunohistochemistry (mIHC) staining for CD8, γH2AX (phosphorylated histone family member X, a marker of DNA damage), cleaved caspase3 (a marker of apoptosis), and Ki67 revealed elevated DNA damage, increased apoptosis, and decreased proliferation in T cells after niraparib treatment (Fig. 1, E to G). Six of 12 individuals exhibited increased γH2AX, elevated cleaved caspase3, and diminished Ki67 staining in $CD8^+$ T cells concurrently after niraparib treatment (Fig. 1, F and G). These patients demonstrated less CA125 reduction, a worse objective response rate (83.33% versus 50%, measured by Response Evaluation Criteria in Solid Tumours version 1.1, RECIST1.1), and a shorter PFS for niraparib treatment (Fig. 1, H and I, and table S1). In summary, using clinical samples from this phase 2 trial, we demonstrated that PARPi monotherapy is associated with reduced proliferation, increased apoptosis, and increased DNA damage in T cells, which may correlate with worse clinical responses and shorter PFS.

PARPis induce T cell growth inhibition, viability loss, and DNA damage

To assess whether the elevated DNA damage in T cells was caused directly by PARPi treatment, three US Food and Drug Administration–approved PARPis for EOC maintenance treatment (olaparib, niraparib, and rucaparib) were used to treat primary human T cells at the maximum serum concentrations (C_{max}) (olaparib, 25 μM; niraparib, 3.75 μM; rucaparib, 8 μM) (*25*) or half of C_{max}. Because niraparib can be enriched three to four times in the TME, a concentration of 10 μM was used (*6*). PARPi treatment decreased proliferation and viability of T cells isolated from healthy donors (Fig. 2A and fig. S1A). After olaparib and niraparib treatment, the proportion of $Ki67^+$ T cells was reduced, and carboxyfluorescein diacetate succinimidyl ester (CFSE) staining also revealed a decrease in mitotic activity (Fig. 2, B and C). PARPi treatment also led to increased terminal deoxynucleotidyl transferase–mediated deoxyuridine triphosphate nick end labeling (TUNEL) staining in T cells (Fig. 2, B and C). Because PARPis induce DNA damage in cancer cells via dsDNA breaks, we hypothesized that the inhibitory effect of PARPis on T cells could be attributed to increased DNA damage. As hypothesized, increased γH2AX was observed by flow cytometry (Fig. 2, B and C), suggesting increased DNA damage. Immunoblotting also revealed increased γH2AX and cleaved caspase3 abundance after PARPi treatment (Fig. 2D). There were also more $TUNEL^+$ cells and $\gamma H2AX^+$ cells by immunofluorescence and an increased number of dsDNA breaks (evaluated through a Comet assay under alkaline conditions) in T cells after olaparib or niraparib treatment (Fig. 2, E and F). Furthermore, loss of cell viability and increased DNA damage were documented in T cells from patients with EOC and different germline *BRCA* mutation statuses after PARPi treatment (fig. S1, B to D).

An RNA expression profile and reverse-phase protein array analysis were then undertaken. Differential gene expression profiles of T cells treated by olaparib or vehicle for 24 hours (fig. S1E and table S2) revealed an enrichment of DNA damage and apoptosis pathways after olaparib treatment (Fig. 2G). Protein array analysis revealed a marked rise in the DNA damage marker γH2AX and apoptosis indicators cleaved caspase3 and cleaved PARP, alongside a reduction in the proliferation marker Ki67 in T cells after PARPi treatment for 24, 48, and 96 hours (Fig. 2H and table S3). Increases in other DNA damage response markers, including p-ATM (phosphorylated ataxia telangiectasia mutated kina), p-ATR (phosphorylated ataxia telangiectasia and Rad3-related kinase), p-CHK1 (phosphorylated checkpoint kinase 1), RAD51 (RAD51 recombinase), and RAD51C (RAD51 paralog C), were also observed after PARPi treatment (fig. S1F).

PARP1 is responsible for PARPi-induced DNA damage in T cells

To uncover the mechanism underlying PARPi-induced DNA damage in T cells, a whole-genome CRISPR-Cas9 (clustered regularly interspaced short palindromic repeats) knockout screen was conducted in human T cells (*26*). T cells from healthy donors were transfected with a genome-scale CRISPR-Cas9 knockout lentivirus library. One day after transfection, Cas9 protein was electroporated into the T cells. Olaparib was then administered at a concentration of 50 μM for 6 days to facilitate positive selection, and the surviving cells were harvested for whole-genome sequencing. The model-based analysis of genome-wide CRISPR-Cas9 knockout (MAGeCK) (*27*) algorithm was used to identify the most frequently knocked-out genes after olaparib treatment. *PARP1* displayed the most significant

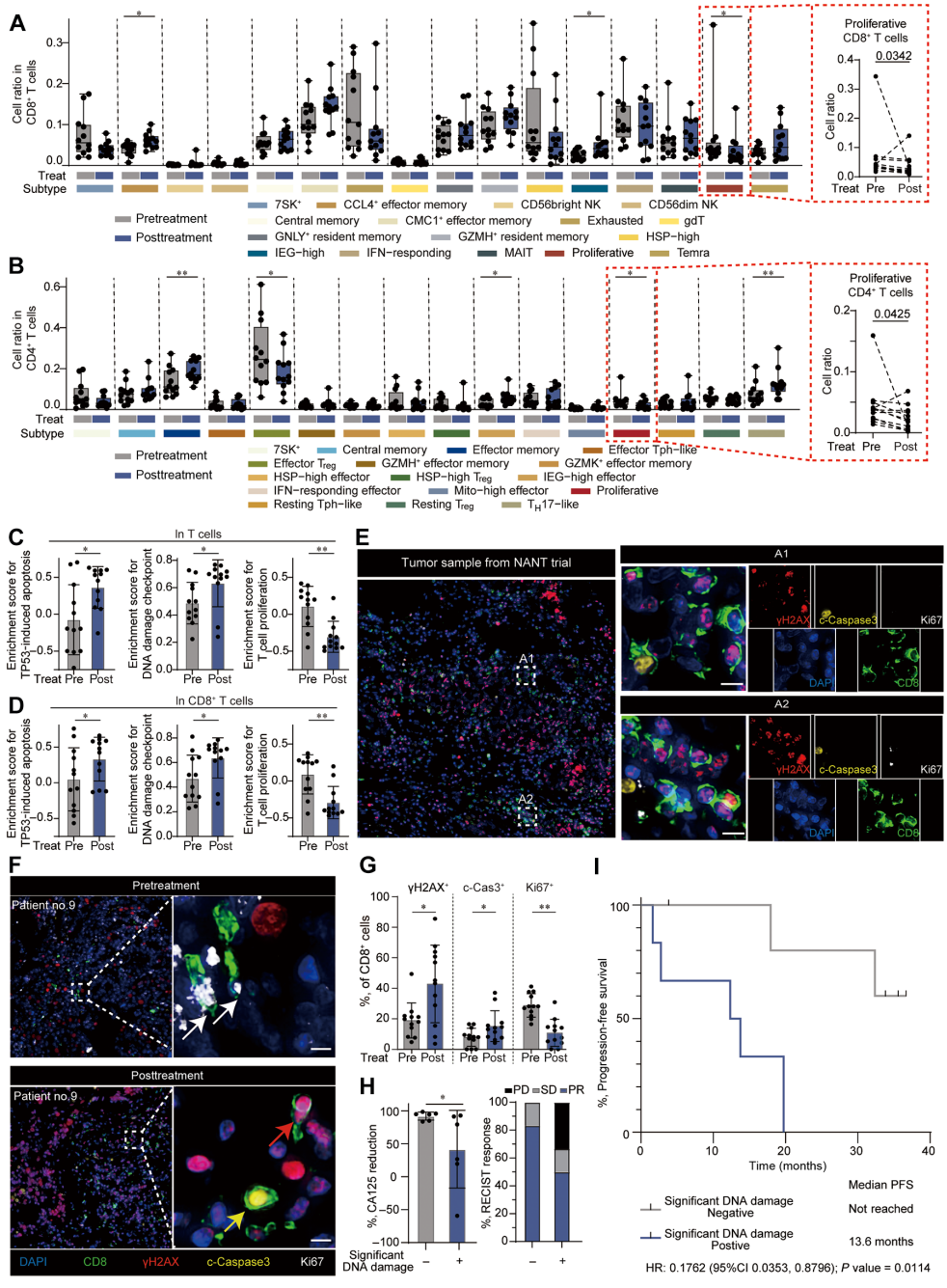

Fig. 1. Identification of DNA damage in T cells in samples after monotherapy with a PARPi. (**A** and **B**) Cell ratio changes for different CD8$^+$ T cell subtypes (A) and CD4$^+$ T cell subtypes (B) identified by scRNA-seq analysis of paired samples taken before and after niraparib treatment. Pretreatment samples (light gray) are plotted on the left, and posttreatment samples (dark blue) are plotted on the right for each T cell subtype. (**C** and **D**) Enrichment scores for apoptosis, DNA damage checkpoint, and T cell proliferation in T cells (C) and CD8$^+$ T cells (D) for each sample. (**E** and **F**) Representative immunofluorescence images of Ki67 (white), cleaved caspase3 (yellow), γH2AX (red), and CD8 (green) staining of a tumor sample obtained after niraparib neoadjuvant treatment (E) and in paired tumor samples obtained before and after niraparib neoadjuvant treatment (F). Nuclei were stained blue with 4′,6-diamidino-2-phenylindole (DAPI). White arrows mark Ki67$^+$CD8$^+$ cells. Yellow arrows mark cleaved caspase3$^+$ CD8$^+$ cells. Red arrows mark γH2AX$^+$ CD8$^+$ cells. A1 and A2 show higher magnification of two representative areas. Scale bars, 5 μm. (**G**) Percentage of CD8$^+$ T cells staining for Ki67$^+$, cleaved caspase3$^+$, or γH2AX$^+$ in patient tumor samples. (**H**) The percentage of CA125 decrease (left) in patients without (light gray) or with (dark blue) substantial DNA damage in CD8$^+$ T cells and RECIST response rate (right) in patients without or with substantial DNA damage in CD8$^+$ T cells. The percentage of CA125 decrease indicates the reduction in serum CA125 concentration after treatment. (**I**) PFS in patients without (light gray) or with (dark blue) significant DNA damage in CD8$^+$ T cells. Twelve patients for comparison. Statistical significance was determined by Wilcoxon signed-rank test [(A) to (D) and (G)], unpaired Student *t* test (H), and log rank (Mantel-Cox) survival test (I). Data are presented as means ± SEM [(A) to (D), (H), and (G)]. GNLY, granulysin; IEG, immediate-early genes; CMC1, C-X9-C motif containing 1; MAIT, mucosal associated invariant T cell; HSP, heat shock proteins; gdT, gamma/delta T cell; T_{ph}, peripheral helper T cell; PD, progressive disease; SD, stable disease; PR, partial response; NK, natural killer; T_{reg}, regulatory T cell; T_H17, T helper cell 17; HR, hazard ratio; CI, confidence interval. *$P < 0.05$ and **$P < 0.01$.

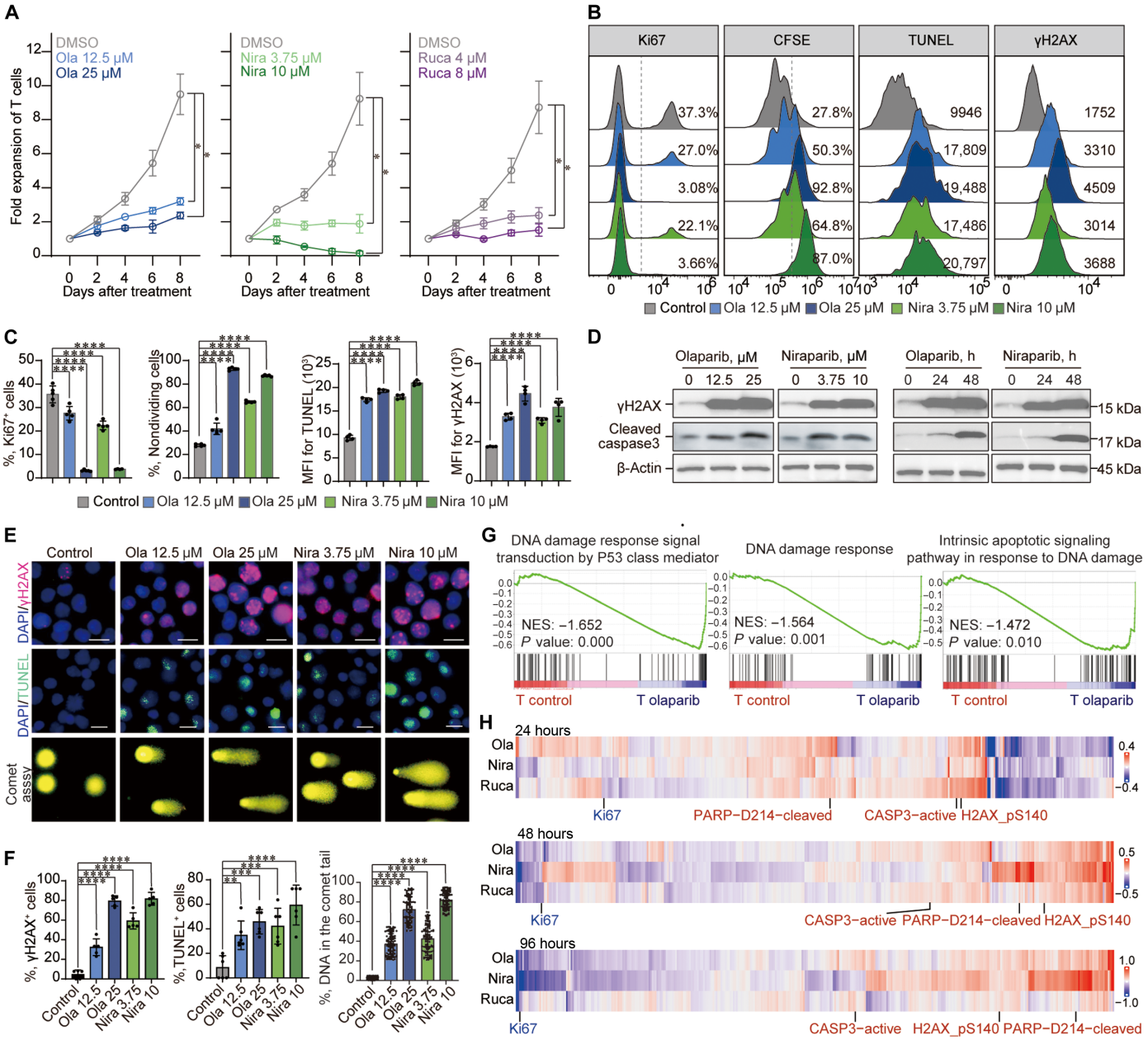

Fig. 2. PARPis induce T cell growth inhibition, viability loss, and DNA damage. (**A**) Expansion curve for T cells in vitro under different concentrations and durations of olaparib (Ola), niraparib (Nira), and rucaparib (Ruca) treatment. (**B**) Representative flow cytometry profiles for Ki67, CFSE, TUNEL, and γH2AX staining in T cells after exposure to different concentrations of olaparib (Ola) and niraparib (Nira) for 48 hours. (**C**) Quantification of percentage of Ki67-positive cells, percentages of cells negative for CFSE, and mean fluorescence intensity (MFI) for TUNEL and γH2AX in T cells after exposure to different concentrations of olaparib or niraparib, from (B). (**D**) Immunoblotting of γH2AX and cleaved caspase3 in T cells after exposure to different concentrations and durations of olaparib and niraparib. (**E**) Representative immunofluorescence images stained for γH2AX (magenta, top), TUNEL (green, middle), and comet assay in T cells after exposure to different concentrations of olaparib (Ola) and niraparib (Nira) for 48 hours (h). Nuclei were stained blue with DAPI in the top two rows. Scale bars, 10 μm. (**F**) Quantification of γH2AX-positive T cells and TUNEL-positive T cells and the percentage of DNA in the comet tail for T cells in accordance with (E). (**G**) Gene set enrichment analysis (GSEA) for pathways enriched in T cells after olaparib exposure for 24 hours. (**H**) RPPA profiles for T cells exposed to olaparib (Ola), niraparib (Nira), or rucaparib (Ruca) for 24, 48, or 96 hours. Red indicates up-regulated proteins after PARPi exposure, whereas blue represents the down-regulated proteins. Three or more biological replicates were performed for each test. Statistical significance was determined by two-way ANOVA (A) or one-way ANOVA [(C) and (F)]. Data are presented as means ± SEM [(A), (C), and (F)]. *$P < 0.05$, **$P < 0.01$, ***$P < 0.001$, and ****$P < 0.0001$. NES, normalized enrichment score; DMSO, dimethyl sulfoxide.

depletion in human T cells after olaparib treatment (Fig. 3A and table S4).

We then conducted in vitro knockout of *PARP1* in T cells for validation. *PARP1* knockout efficiency was confirmed at the genomic (fig. S2A), protein (Fig. 3B), and functional (fig. S2B) levels. *PARP1* knockout attenuated DNA damage, apoptosis, loss of viability, and reversed inhibition of expansion in T cells after olaparib exposure (Fig. 3, B to D). Flow cytometry (Fig. 3, E and F), immunofluorescence, and Comet assays (Fig. 3, G and H) all supported reduced DNA damage, apoptosis, and dsDNA in T cells with knockout of *PARP1* after olaparib treatment. In T cells with germline *BRCA1* (Fig. 3I and fig. S2, C and D) and *BRCA2* (Fig. 3I and fig. S2, E and F)

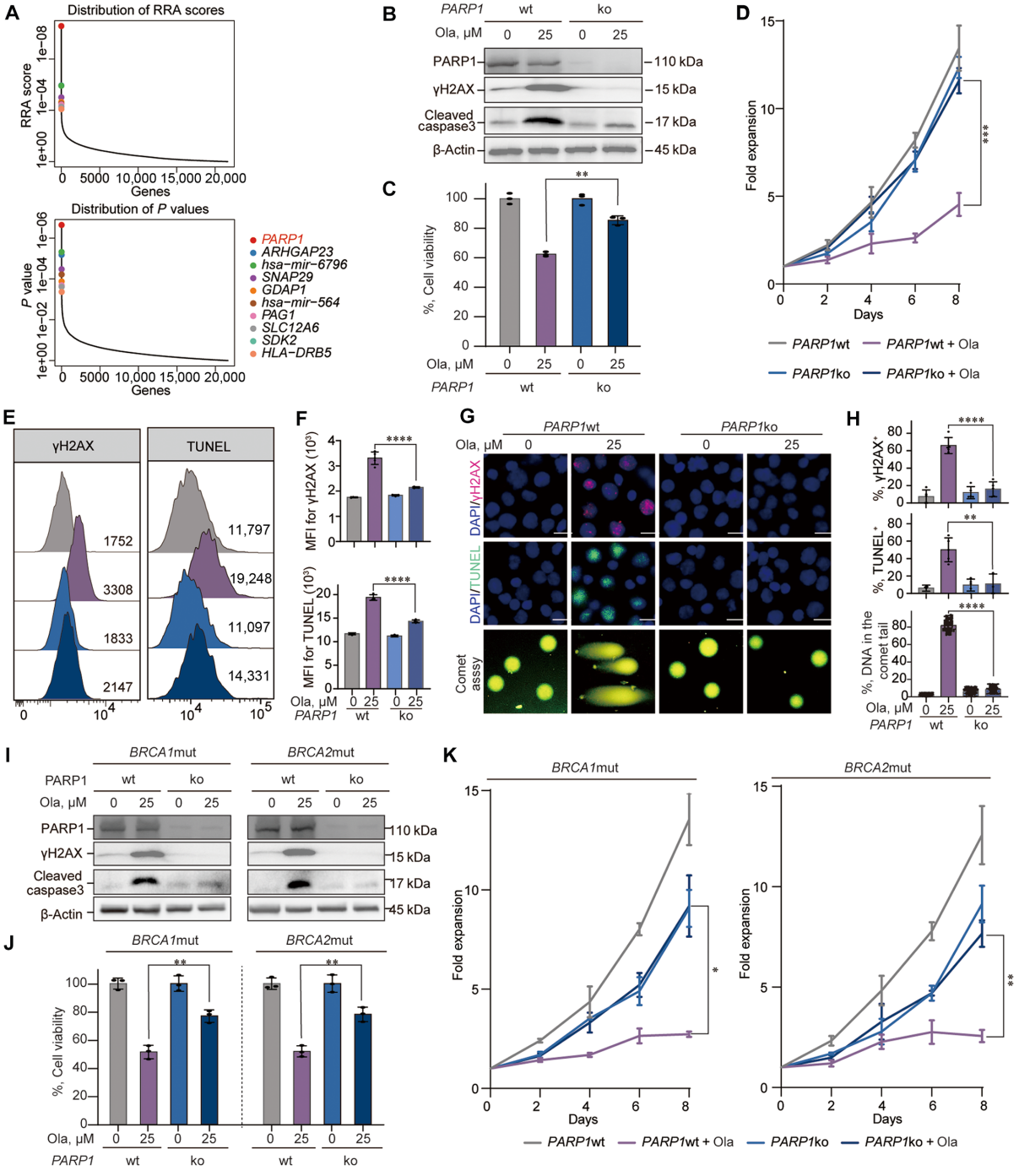

Fig. 3. PARP1 is responsible for PARPi-induced DNA damage in T cells. (**A**) The genes enriched after olaparib treatment, ranked by RRA score (top) or *P* values (bottom). (**B**) Immunoblots of γH2AX and cleaved caspase3 abundance in T cells with *PARP1* wild-type (*PARP1*wt) and *PARP1* knockout (*PARP1*ko) after olaparib (Ola) exposure for 48 hours. (**C**) Cell viability measured by propidium iodide staining in T cells with *PARP1*wt and *PARP1*ko after olaparib (Ola) exposure for 48 hours. (**D**) Expansion curves for T cells with *PARP1*wt or *PARP1*ko under olaparib (Ola) exposure. (**E**) Representative flow cytometry profiles for γH2AX and TUNEL staining in T cells with *PARP1*wt or *PARP1*ko after olaparib (Ola) exposure for 48 hours. (**F**) MFI of γH2AX and TUNEL staining of T cells, from (E). (**G**) Representative immunofluorescence images for γH2AX (magenta, top row), TUNEL staining (green, middle row), and comet assay (yellow, bottom row) in T cells with *PARP1*wt and *PARP1*ko after olaparib (Ola) exposure for 48 hours. Nuclei were stained blue with DAPI in the top two rows. Scale bars, 10 μm. (**H**) Quantification of γH2AX and TUNEL-positive T cells and the percentage of DNA in the comet tail for T cells in accordance with (G). (**I**) Immunoblots of γH2AX and cleaved caspase3 abundance in T cells with *PARP1*wt and *PARP1*ko after olaparib (Ola) exposure for 48 hours. (**J**) Cell viability measured by PI staining in T cells with *PARP1*wt and *PARP1*ko after olaparib (Ola) exposure for 48 hours. (**K**) Expansion curves for T cells with *PARP1*wt and *PARP1*ko under olaparib (Ola) exposure. [(A) to (H)] T cells were obtained from healthy donors. [(I) to (K)] T cells were obtained from patients with EOC with germline *BRCA1* or *BRCA2* mutations. Three biological replications were performed for each experiment. Statistical significance was assessed by one-way ANOVA [(C), (F), (H), and (J)] or two-way ANOVA [(D) and (K)]. Data are presented as means ± SEM [(C), (D), (F), (H), (J), and (K)]. **P* < 0.05, ***P* < 0.01, ****P* < 0.001, and *****P* < 0.0001.

mutations, knockout of *PARP1* also reduced DNA damage, apoptosis, and proliferation loss in response to olaparib treatment (Fig. 3, I to K).

We used the selective PARP1 inhibitor AZD5305 to further test the role of PARP1 during T cell DNA damage. AZD5305 led to a dose-dependent loss of cell viability in T cells (fig. S3, A and B), along with inhibition of expansion and increased DNA damage and apoptosis (fig. S3, C to F), all of which were attenuated by knockout of *PARP1* (fig. S3, B to F). Because olaparib targets both PARP1 and PARP2, we knocked out *PARP2* (fig. S3G); however, this did not attenuate the effects of olaparib on T cells in vitro (fig. S3, H to L).

Introduction of mutations to *PARP1* in T cells diminishes PARPi-induced DNA damage

Mutations in *PARP1* around the sites connecting the ZnF (Zinc finger), WGR (tryptophan-glycine-arginine–rich), and the regulatory helical domain (HD) have been reported to increase cancer cell resistance to PARPis by decreasing PARP1-DNA binding and PARP1 trapping (*28*, *29*). We therefore introduced nonsynonymous mutations in *PARP1* in primary human T cells at these sites via cytosine base editing to assess whether PARPi-induced DNA damage to T cells could be alleviated (*30*).

Nine single guide RNAs (sgRNAs) targeting *PARP1* at sites around the center connecting ZnF-WGR-HD domains were designed, with two targeting the DNA binding site of the ZnF domain (M43-D45, referred to as D45-sg1 to sg2), four targeting points contacting the WGR domain with the ZnF domain (S588-R591, referred to as S588-sg1 to sg4), and three targeting interaction sites that bridge the DNA binding domain and the catalytic domain (D743-G745, referred to as G745-sg1 to sg3) (Fig. 4A). Each of these sgRNAs was electroporated into activated human T cells individually, together with CBE3 (cytosine base editor 3) protein to achieve point mutations. Genomic DNA was extracted 3 days after electroporation, and Sanger sequencing was performed to validate the genomic changes (fig. S4A) (*31*). After confirming the genomic alterations in these *PARP1*-engeniered T cells, we evaluated the expansion ability of the engineered T cells (Fig. 4B) and their resistance to a PARPi in vitro (Fig. 4C).

Among the nine sgRNAs, D45-sg1, S588-sg2, and G745-sg2 were selected for further investigation. For these three sgRNAs, D45-sg1 resulted in D45N and M43I mutations, both estimated to occur in more than 75% of the edited cells. S588-sg2 mainly resulted in an S588F mutation, estimated to occur in more than 80% of the cells. G745-sg2 led to G745K mutation (estimated to occur in more than 60% of cells), G745R mutation (estimated to occur in less than 20% of cells), or G745E mutation (estimated to occur in more than 20% of cells) (fig. S4A). The T cells edited with these sgRNAs were designated as T_{D45}, T_{S588}, and T_{G745} cells, respectively. Compared with T cells electroporated with a scaffold sgRNA (T_{NC}), all T cells carrying *PARP1* mutations exhibited increased resistance to olaparib (Fig. 4D) and reduced DNA damage and apoptosis under olaparib treatment as measured by immunoblotting (fig. S4B), flow cytometry, and immunofluorescence (Fig. 4, E to H).

The immune phenotypes of T_{D45}, T_{S588}, and T_{G745} cells were also compared with that of T_{NC} cells. *PARP1* mutations did not substantially alter the ratios of $CD8^+$ and $CD4^+$ T cells (fig. S4C). The proportion of naïve ($CCR7^+$ $CD45RO^-$), central memory ($CCR7^+$ $CD45RO^+$), effector memory ($CCR7^-$ $CD45RO^+$), and terminally differentiated effector memory ($CCR7^-$ $CD45RO^-$) T cells was also similar among T_{NC}, T_{D45}, T_{S588}, and T_{G745} cells (fig. S4D). Assessment of T cell activation markers, including CD38, CD69, and HLA-DR, showed no disparities among T_{D45}, T_{S588}, T_{G745}, and T_{NC} cells (fig. S4E). There were also no differences in interferon-γ (IFN-γ), tumor necrosis factor–α (TNF-α), or interleukin-2 (IL-2) production between T cells with and without *PARP1* mutations after stimulation with PMA (phorbol 12-myristate 13-acetate) and ionomycin for 4 hours (fig. S4F).

Alleviating PARPi-induced DNA damage in T cells enhances tumor response to PARPi treatment, either as monotherapy or in combination with ICI

To investigate whether the reduction of PARPi-induced DNA damage in T cells could result in enhanced antitumor immunity mediated by PARPis, we conditionally introduced one *Parp1* mutation mentioned above ($Parp1^{S588F}$) in T cells using T cell–specific cre-expressing mice (CD4-cre; $Parp1^{S588F/\ S588F}$ mice, referred to as $Thy^{\Delta Parp1\text{-}S588F}$), in comparison with cre-negative mice ($Parp1^{S588F/\ S588F}$ mice, referred to as $Thy^{Parp1+/+}$) (fig. S5, A and B). T cells isolated from $Thy^{\Delta Parp1\text{-}S588F}$ mice exhibited reduced DNA damage and apoptosis in response to olaparib treatment (fig. S5C). *Trp53*$^{-/-}$ *Brca1*$^{-/-}$ ID8 cells were intraperitoneally injected to establish an advanced EOC model (Fig. 5A).

After olaparib treatment, a reduction in tumor burden was observed in $Thy^{\Delta Parp1\text{-}S588F}$ mice compared with the $Thy^{Parp1+/+}$ controls (Fig. 5, B and C). Increased $CD8^+$ T cell counts were noted in the TME of $Thy^{\Delta Parp1\text{-}S588F}$ mice after olaparib treatment (Fig. 5D and fig. S5D), accompanied by improved T cell proliferation and reduced T cell DNA damage compared with that in $Thy^{Parp1+/+}$ mice (Fig. 5, E to G, and fig. S5E). Similar findings were observed in $CD8^+$ T cells in the spleens of tumor-bearing $Thy^{\Delta Parp1\text{-}S588F}$ mice treated with olaparib (fig. S5, F to I). Immunohistochemistry staining for CD8 demonstrated increased $CD8^+$ T cell infiltration into tumors (Fig. 5, H and I), and immunofluorescence staining demonstrated reduced γH2AX staining in $CD8^+$ T cells, indicating reduced DNA damage after PARPi treatment in $Thy^{\Delta Parp1\text{-}S588F}$ mice (Fig. 5, J and K). Olaparib treatment was also associated with increased granzyme B^+ and IFN-γ^+ $CD8^+$ cells and decreased $PD1^+$ $TIM3^+$ $CD8^+$ T cells in tumor-bearing $Thy^{\Delta Parp1\text{-}S588F}$ mice but not tumor-bearing $Thy^{Parp1+/+}$ mice (fig. S6A). No significant organ abnormalities were found in either $Thy^{\Delta Parp1\text{-}S588F}$ or $Thy^{Parp1+/+}$ mice before or after olaparib treatment (fig. S6B). Depletion of $CD8^+$ T cells through administration of an anti-CD8 antibody at the time of tumor cell injection and during treatment eliminated the improved antitumor efficacy seen in $Thy^{\Delta Parp1\text{-}S588F}$ mice treated with a PARPi (fig. S6, C and D). Together, these results indicated that alleviating PARPi-induced DNA damage in T cells could increase PARPi efficacy by enhancing T cell–mediated antitumor immunity.

To investigate whether alleviating PARPi-induced DNA damage in T cells improves combination therapy with ICI, olaparib and anti-PD1 monoclonal antibodies (clone: RMP1-14) were concurrently administered to the advanced EOC syngeneic mouse models (olaparib, once daily; anti-PD1, twice weekly) which were established by intraperitoneal injection of *Trp53*$^{-/-}$ *Brca1*$^{-/-}$ ID8 cells. Treatments started 7 days after tumor cell implantation. The combination resulted in improved control of tumor burden in $Thy^{\Delta Parp1\text{-}S588F}$ mice

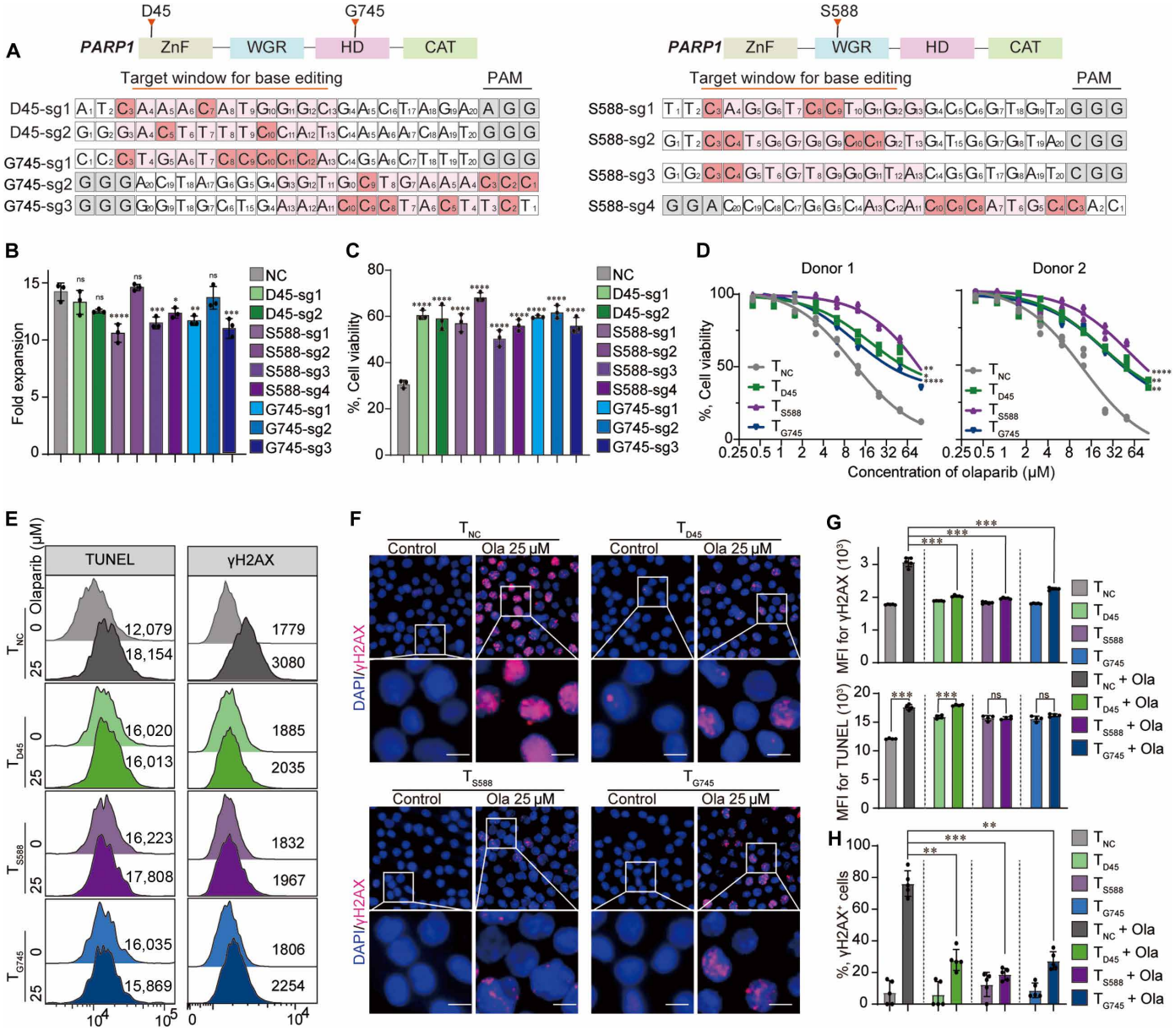

Fig. 4. Mutations in *PARP1* diminish PARPi-induced DNA damage in T cells. (**A**) Sequence of sgRNAs and their general targeting position on *PARP1*, with edits to the ZnF-HD domain region shown at the left and edits to the WGR domain region at the right. The general position of the edits in each region is indicated in the *PARP1* schematic above each group. The specific sgRNA for each edit is named to the left. Light red indicates that the base was within the window of editing for each sgRNA. Deep red indicates that the base was changed. (**B**) The fold expansions for T cells with different point mutations on *PARP1* for 9 days. (**C**) Cell viability measured by propidium iodide staining for T cells after olaparib exposure for 72 hours. (**D**) Cell viability measured by propidium iodide staining for T_{NC}, T_{D45}, T_{S588}, and T_{G745} cells after exposure to different concentrations of olaparib for 72 hours. (**E**) Representative flow cytometry profiles for TUNEL and γH2AX staining in T_{NC}, T_{D45}, T_{S588}, and T_{G745} cells after exposure to olaparib for 48 hours. (**F**) Representative immunofluorescence images for γH2AX foci in T_{NC}, T_{D45}, T_{S588}, and T_{G745} cells after exposure to olaparib for 48 hours. Scale bars, 5 μm. (**G**) MFI of TUNEL and γH2AX from (E). (**H**) Quantification of γH2AX-positive cells, related to (F). Three or more biological replications were used for each test. Statistical significance was determined by one-way ANOVA [(B), (C), (G), and (H)] or two-way ANOVA (D). Data are presented as means ± SEM [(B), (C), (D), (G), and (H)]. $*P < 0.05$, $**P < 0.01$, $***P < 0.001$, and $****P < 0.0001$; ns, not significant. PAM, protospacer adjacent motif.

compared with $Thy^{Parp1+/+}$ mice, as assessed by in vivo imaging (Fig. 5, L and M), resulting in improved survival for $Thy^{\Delta Parp1\text{-}S588F}$ mice compared with $Thy^{Parp1+/+}$ mice (Fig. 5N). Together, these data support the concept that alleviating DNA damage in T cells improves the efficacy of PARPis as monotherapy and in combination with ICI.

PARP1-engineered CAR T cells experience less DNA damage and exhibit superior antitumor activity during PARPi treatment

CAR T cells targeting mesothelin have demonstrated promising antitumor activity in EOC, and the combination of PARPis and CAR T therapies may further enable synergistic efficacy (*24*, *32*). We

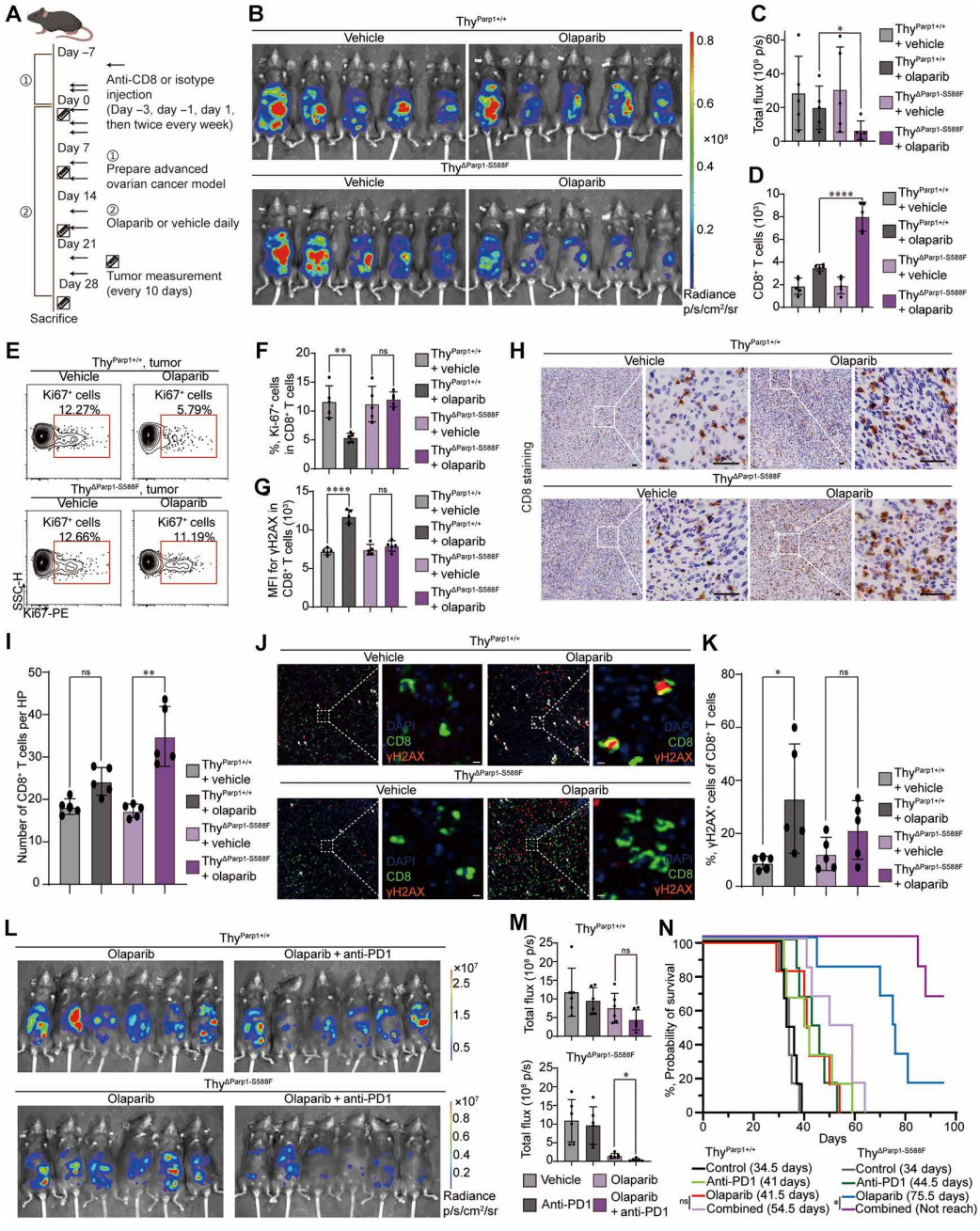

Fig. 5. Minimizing PARPi-induced DNA damage in T cells enhances the efficiency of a PARPi alone and in combination with ICI. (**A**) Flowchart for ID8-bearing mice models. *Trp53*$^{-/-}$ *Brca1*$^{-/-}$ ID8 cells were intraperitoneally injected to establish an advanced EOC model at day −7, and anti-CD8 or isotype was injected at day −3, day −1, and day 1, and then twice every week. Olaparib and vehicle were administered orally daily. (**B**) In vivo bioluminescence images showing tumor volumes after treatment with vehicle or olaparib in Thy$^{Parp1+/+}$ or Thy$^{\Delta Parp1\text{-}S588F}$ at the end of the study. (**C**) Quantification of tumor burden by luminescence for mice in (B). (**D**) Quantification of tumor-infiltrating CD8$^+$ T cell numbers for mice receiving isotype antibody measured by flow cytometry. (**E**) Representative flow cytometry indicating Ki67$^+$ CD8$^+$ T cells in tumors without (left) and with (right) olaparib treatment from Thy$^{Parp1+/+}$ mice (top) and Thy$^{\Delta parp1\text{-}S588F}$ mice (bottom). (**F**) Quantification of percentage of Ki67$^+$CD8$^+$ T cells in (E). (**G**) Quantification of γH2AX in CD8$^+$ T cells in tumors from Thy$^{Parp1+/+}$ or Thy$^{\Delta parp1\text{-}S588F}$ mice, treated with vehicle or olaparib, measured by flow cytometry. (**H**) Representative immunohistochemistry staining for CD8 of tumors from Thy$^{Parp1+/+}$ mice (top) and Thy$^{\Delta parp1\text{-}S588F}$ mice (bottom) treated with vehicle or olaparib for 28 days. Scale bars, 50 μm. (**I**) Quantification of CD8$^+$ T cell numbers in (H). (**J**) Representative immunofluorescence staining for γH2AX (orange) and CD8 (green) of tumors from Thy$^{Parp1+/+}$ mice (top) and Thy$^{\Delta parp1\text{-}S588F}$ mice (bottom) treated with vehicle or olaparib for 28 days. Scale bars, 5 μm. (**K**) Quantification of percentage of γH2AX-positive CD8$^+$ T cells in (J). (**L**) In vivo bioluminescence images showing tumor burden in Thy$^{Parp1+/+}$ mice (top) and Thy$^{\Delta Parp1\text{-}S588F}$ mice (bottom) after olaparib or combination of olaparib plus anti-PD1 monoclonal antibody treatment. (**M**) Quantification of tumor burden as monitored by luminescence intensity for mice receiving olaparib or a combination of olaparib and anti-PD1 monoclonal antibody treatment, as shown in (L). (**N**) Kaplan-Meier survival curves of mice in the indicated treatment groups. Five mice each group [(A) to (K)]. Six mice for each group [(L) to (N)]. Statistical significance was determined by one-way ANOVA [(C), (D), (F), (G), (I), (K), and (M)] or log-rank (Mantel-Cox) survival test (N). Data are presented as means ± SEM [(C), (D), (F), (G), (I), (K), and (M)]. *$P < 0.05$, **$P < 0.01$, and ****$P < 0.0001$. PE, phycoerythrin.

hypothesized that CAR T cells also experienced DNA damage when coadministered with PARPis, and mitigating PARPi-induced DNA damage by engineering *PARP1* could improve the tumor eradication potential of combination therapy.

We generated CAR T cells following protocols from our previous clinical trial (NCT05141253) and engineered *PARP1* with D45-sg1, S588-sg2, and G745-sg2. These *PARP1*mut CAR T cells were designated as CAR-T_{D45}, CAR-T_{S588}, and CAR-T_{G745} cells, respectively (Fig. 6A and fig. S7A). The *PARP1* mutations were effectively incorporated, achieving a C-T conversion rate exceeding 90% for CAR-T_{D45} and CAR-T_{S588} and more than 60% for CAR-T_{G745} (fig. S7B). The *PARP1*mut CAR T cells demonstrated improved cell viability (Fig. 6B) and decreased γH2AX and TUNEL staining (Fig. 6C) after olaparib treatment, indicating that the mutations mitigated PARPi-induced DNA damage.

Ovarian cancer cell lines, including OVCAR8, SKOV3, and OVCAR3, were used to assess the in vitro tumor-killing capacities of these *PARP1*mut CAR T cells in the presence and absence of olaparib (fig. S7C). IFN-γ and TNF-α secretion from CAR T_{NC} cells exhibited a time-dependent decline upon olaparib exposure, whereas cytokine production in *PARP1*mut CAR T cells remained unaffected (Fig. 6D). The in vitro killing efficiency of CAR T_{NC} cells also decreased significantly when cocultured with olaparib, which was not observed in *PARP1*mut CAR T cells (Fig. 6E and fig. S7D).

Next, the antitumor efficacy of *PARP1*mut CAR T cells during PARPi cotreatment was evaluated in vivo using SKOV3 cell–derived xenograft (CDX) mouse models. CDX models were established by subcutaneously inoculating 5×10^6 SKOV3 cells into NSG mice. CAR-T_{NC}, CAR-T_{D45}, and CAR-T_{S588} cells were administered intravenously once tumors reached a volume of 200 mm^3. Olaparib was orally administered at a daily dose of 100 mg/kg after CAR–T cell infusion. Results showed that CAR-T_{NC}, CAR-T_{D45}, and CAR-T_{S588} cells alone resulted in tumor remission in approximately 40% of mice (Fig. 6F). The inclusion of olaparib marginally reduced tumor volume but did not notably affect the tumor control rate for CAR-T_{NC} cells. Nevertheless, the combination of olaparib with CAR-T_{D45} and CAR-T_{S588} treatment effectively inhibited tumor progression in nearly all mice (Fig. 6F), resulting in a markedly extended survival period (Fig. 6G). Particularly in the case of CAR-T_{S588} cells, complete eradication of tumors was observed for all seven mice when combined with olaparib (Fig. 6F), leading to long-term tumor-free survival (Fig. 6G), without evidence of toxicity (fig. S8A). Furthermore, gallium-68–labeled granzyme B–specific positron emission tomography (PET)/computed tomography imaging of T cells in vivo demonstrated elevated granzyme B in tumors cotreated with CAR-T_{S588} and olaparib, indicating an increase in cytotoxic T cells in the TME (Fig. 6, H and I, and fig. S8B). In summary, these in vitro and in vivo studies demonstrated that when cotreated with PARPis, CAR T cells exhibited improved tumor-killing ability when PARPi-induced DNA damage was reduced.

Coadministration of *PARP1*mut CAR T cells and a PARPi improves efficacy against EOC in PDX models

To further investigate the therapeutic potential of *PARP1*-engineered CAR T cells and PARPis in EOC, adaptive transfer of CAR-T_{S588} combined with olaparib treatment was used in two EOC patient-derived xenograft (PDX) models with different genetic backgrounds, one established from a patient with a newly diagnosed HRD tumor (HRD-PDX) and the other established from a patient with EOC after second recurrence (multiple-relapse PDX, MR-PDX), to simulate both treatment-naive and tumor relapse scenarios. The presence of mesothelin on cancer cells was validated using flow cytometry (fig. S8, C and D).

The HRD tumor sample was obtained from a patient with EOC during primary debulking surgery before any treatment. In the HRD-PDX model, CAR T cell and olaparib administration followed a protocol similar to the CDX model. When used individually, CAR-T_{S588} and CAR-T_{NC} cells exhibited comparable antitumor effects. Addition of olaparib did not significantly improve the efficacy of CAR-T_{NC} cells, whereas the combination of CAR-T_{S588} cells and olaparib did significantly improve treatment efficacy ($P < 0.05$; Fig. 7A), associated with reduced tumor weights and smaller tumor volumes at the end of the study (Fig. 7, B and C), and increased $CD8^+$ tumor-infiltrating lymphocytes by immunohistochemistry staining for CD8 (Fig. 7D). Improved proliferation and decreased DNA damage were seen in CAR-T_{S588} cells after olaparib treatment, as compared with CAR-T_{NC} cells (Fig. 7, E and F, and fig. S8, E and F).

The MR tumor specimen was obtained from the patient during the debulking surgery for the patient's second cancer recurrence after second-line chemotherapy and 16 months of olaparib maintenance therapy (Fig. 7G). In the MR-PDX model, combination treatment slowed tumor growth curve, reduced tumor volumes, and reduced tumor weights compared with CAR-T_{S588} cells alone, whereas the addition of olaparib did not alter the efficacy of CAR-T_{NC} cells (Fig. 7, H to K). Olaparib increased CAR T cell numbers in the tumors of CAR-T_{S588}–and–olaparib–treated animals (Fig. 7L), associated with increased Ki67 and decreased γH2AX compared with CAR-T_{NC} cells (Fig. 7, M and N). Increased $CD8^+$ T cell infiltration and reduced DNA damage for CAR-T_{S588} and PARPi cotreatment were also tested using immunohistochemistry (fig. S8G) and mIHC staining (Fig. 7O and fig. S8H).

DISCUSSION

In this study, we demonstrated that relieving DNA damage suffered by T cells during PARPi treatment could enhance the efficacy of PARPis, either as monotherapy or in combination with ICIs. We also engineered PARPi-tolerant CAR T cells that demonstrated superior antitumor efficacy when coadministered with PARPis in CDX and PDX models, offering a potentially translatable strategy to potentiate PARPi treatment.

The generation of PARPi-tolerant CAR T cells not only validated our hypothesis that reducing DNA damage caused by PARPis could markedly enhance antitumor immunity but also may serve as a strategy for future clinical translation. CAR T cell therapies have achieved impressive efficacy in hematological malignancies (*33*, *34*). However, their applications in solid tumors are largely hindered by the lack of tumor-specific antigens, impaired tumor infiltration, and the immunosuppressive TME (*35*). Combining CAR T cells with targeted therapies with immune-evoking abilities, such as those featured by PARPis, may be a promising approach to facilitate the clinical application of CAR T cells in solid tumors. The first step would be to ensure CAR T cell expansion and persistence during PARPi treatment (*24*). Our study provided a promising strategy by developing PARPi-tolerant CAR T cells via *PARP1* engineering, which demonstrated improved antitumor activity when cotreated with PARPi. The combination of *PARP1*-engineered CAR T cells and

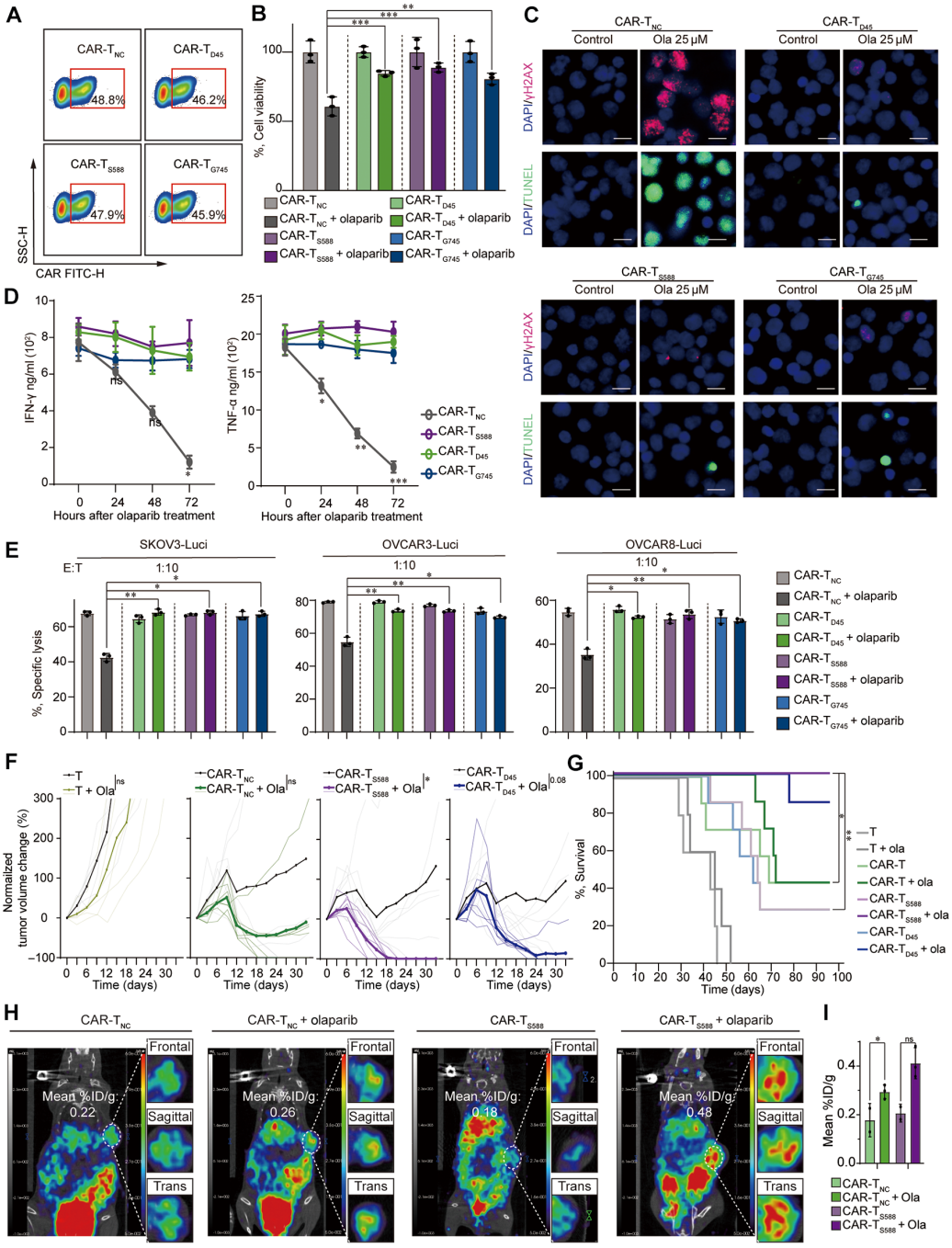

Fig. 6. CAR T cells edited to sustain reduced DNA damage have superior antitumor activity during PARPi treatment. (**A**) Representative flow cytometry staining profiles for CAR expression in CAR-T_{NC}, CAR-T_{D45}, CAR-T_{S588}, and CAR-T_{G745} cells. (**B**) Cell viability measured by propidium iodide staining for CAR-T cells with different point mutations after exposure to olaparib for 48 hours. (**C**) Representative immunofluorescence staining for γH2AX (magenta) and TUNEL staining (green) for CAR-T_{NC}, CAR-T_{D45}, CAR-T_{S588}, and CAR-T_{G745} cells before and after exposure to olaparib. Nuclei were stained blue with DAPI. Scale bars, 10 μm. (**D**) IFN-γ (left) and TNF-α (right) concentrations in the supernatant for CAR-T_{NC}, CAR-T_{D45}, CAR-T_{S588}, and CAR-T_{G745} cells when cocultured with OVCAR8 cells for 6 hours at an effector versus target ratio (E:T) of 1:1, after the exposure to olaparib 25 μM for 24, 48, and 72 hours, compared with 0 hours. (**E**) Percentage of tumor cell lysis for the indicated ovarian cancer cell lines by CAR-T_{NC}, CAR-T_{D45}, CAR-T_{S588}, and CAR-T_{G745} cells when cotreated with olaparib for 24 hours. The lysis rate was normalized by cancer cell numbers under the same concentration of olaparib alone. (**F**) Normalized tumor volume growth curve for SKOV3-CDX models. (**G**) Kaplan-Meier survival curve of SKOV3-CDX mice models. (**H**) Representative images of gallium-68–labeled granzyme B–specific PET imaging. (**I**) Quantitative analysis for gallium-68–labeled granzyme B–specific PET imaging (two mice for the CAR-T_{NC} and CAR-T_{S588} cell group, three mice for the CAR-T_{NC} + Ola and CAR-T_{S588} + Ola group). Three or more biological replicates were performed for each test. Five mice for the T and T + Ola group and seven mice for other groups [(F) and (G)]. Statistical significance was determined by one-way ANOVA [(B), (E), and (I)], two-way ANOVA [(D) and (F)], or log-rank (Mantel-Cox) survival test (G). Data are presented as means ± SEM [(B), (E), and (I)]. *$P < 0.05$, **$P < 0.01$, and ***$P < 0.001$. %ID/g, percentage of total injection dose per gram.

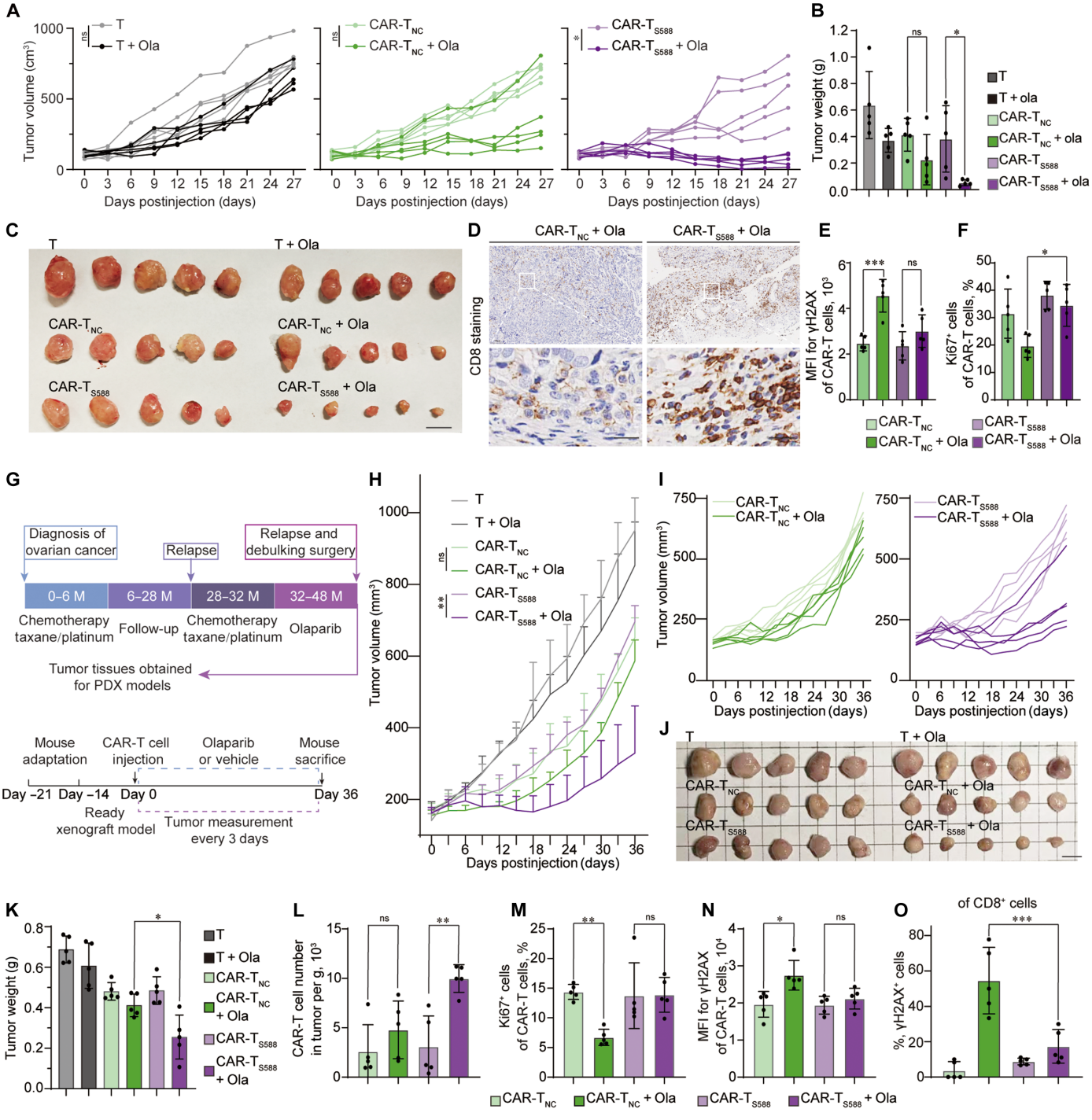

Fig. 7. In PDX models, PARPi-resistant CAR-T cells have improved efficacy with a PARPi. (**A**) Tumor volume growth curves for HRD-PDX models, with T cells with or without olaparib shown on the left, CAR-T_{NC} cells with or without olaparib shown in the middle, and CAR-T_{S588} cells with or without olaparib shown on the right. (**B**) Quantification of tumor weights per the indicated groups. (**C**) Tumor sizes at the end of the experiment for each group. Scale bar, 1 cm. (**D**) Representative immunohistochemistry images stained for CD8 for the CAR-T_{NC} + olaparib and CAR-T_{S588} + olaparib group. Scale bars, 20 μm. (**E** and **F**) Quantitative analysis of γH2AX (E) and Ki67 (F) in CAR-T cells measured by flow cytometry. (**G**) Schematic for MR-PDX model showing the patient's timeline and treatment course, as well as the experimental timeline. (**H**) Tumor volume growth curve for the MR-PDX model. (**I**) Tumor volume growth curve for each mouse in the CAR-T_{NC} versus CAR-T_{NC} + olaparib groups and CAR-T_{S588} versus CAR-T_{S588} + olaparib groups. (**J**) Tumor sizes at the end of the experiment for each group. Scale bar, 1 cm. (**K**) Quantitative analysis for tumor weights per group. (**L**) Quantification of tumor infiltration by CAR-T cells as measured by flow cytometry. (**M**) Quantification of $Ki67^+$ and γH2AX in CAR-T cells in mouse tumors as measured by flow cytometry. (**N**) Quantification of γH2AX in CAR-T cells in mouse tumors as measured by flow cytometry. (**O**) Quantification of percentage of γH2AX-positive $CD8^+$ T cells in mouse tumors by immunofluorescence staining. Significance was determined by two-way ANOVA [(A) and (H)] or one-way ANOVA [(B), (E), (F), (K) to (N), and (O)]. Data are presented as means ± SEM [(B), (E), (F), (H), (K) to (N), and (O)]. $^*P < 0.05$, $^{**}P < 0.01$, and $^{***}P < 0.001$.

PARPis resulted in improved tumor control even in PDXs derived from a heavily pretreated recurrent EOC tumor, highlighting *PARP1* engineering as a promising approach to protect CAR T cells from PARPi-induced DNA damage, thereby maximizing the benefits of combination therapy.

Although PARPis induced T cell DNA damage and proliferation loss, the antitumor efficacy of $CD8^+$ T cells was only restricted, not eliminated. Olaparib treatment did not result in reduced T cell infiltration or T cell activation (including IFN-γ and granzyme B production), which is consistent with previous studies (*36*). These observations could be attributed to the fact that PARPis promote cancer cells to release proinflammatory cytokines rather than directly affecting T cells (*15*). Antitumor T cells recruited and activated by PARPis are potentially more vulnerable to DNA damage than T cells without activation because of their rapid proliferation during activation and cytotoxicity (*37*). In a previous study, treatment with olaparib resulted in significant inhibition of AT3 tumors in immunocompromised mice; however, this antitumor activity is absent in immunocompetent mice, implying that PARPis may exert an unfavorable influence on antitumor T cells (*38*). Previous studies have reported that knockout of *Parp1* in T cells results in enhanced antitumor activity because of increased memory T cells, which disappeared during olaparib treatment because of olaparib's effect on *Parp2* (*38*, *39*). Here, we found that mutations at the DNA trapping sites of *PARP1* lead to enhanced T cell survival during PARPi treatment, which could explain their observation of unfavorable influence of olaparib on antitumor T cells. We did not observe changes in memory T cells, which could be because *PARP1* was mutated rather than knocked out in our study.

This study does have some limitations. First, the NANT clinical trial has not been completed, and the long-term impact of PARPi-induced DNA damage in T cells on treatment efficacy will need to be further evaluated. Second, although our focus was primarily on the effects of PARPis on T cells, the potential impacts of PARPis on other immune cells within the TME remain to be elucidated. For example, in a previous study, PARPis enhanced both the antitumor and protumor characteristics of macrophages via glucose and lipid metabolic reprogramming in breast cancer susceptibility gene (BRCA)–associated triple-negative breast cancers, thereby influencing antitumor T cells (*40*). Third, T cells used in this study did not experience chemotherapy before in vitro PARPi treatment, which is different from regular clinical settings; how T cells that experienced prior chemotherapy respond to PARPis also needs to be explored in future studies.

In conclusion, we identified PARPi-induced DNA damage in T cells as a potential therapeutic opportunity to augment the antitumor efficacy of PARPis, either as monotherapy or in combination with ICIs. In addition, we developed *PARP1*-engineered CAR-T cells that were resistant to PARPi-induced DNA damage and more successfully controlled EOC tumors when combined with PARPi treatment, highlighting a potentially translational strategy for further study.

MATERIALS AND METHODS

Study design

The aim of this study was to assess the effect of PARPis on T cells directly. For human biospecimens, all samples were collected with prior patient consent. Peripheral blood mononuclear cells (PBMCs) were banked during enrollment in NCT04507841. The clinical trial from which specimens were analyzed was approved by the ethics committee of Tongji Medical College, Huazhong University of Science and Technology (S122-5). In controlled laboratory experiments, more than five mice were used in each treatment group. Mice were randomized after tumor establishment for the different treatments. Tumor growth experiments had a predetermined end point based on tumor burden. For each experiment, mouse numbers, statistical tests, and experimental replicates are described in the figure legends. In vitro experiments were repeated at least three times, and the studies were not blinded. No data outliers were excluded. This study was approved by the institutional review board of Tongji Hospital, Tongji Medical College, Huazhong University of Science and Technology (T1-202407087).

Cell lines

The human ovarian cancer cell lines SKOV3 (catalog no. HTB-77) and OVCAR3 (catalog no. HTB-161) were procured from American Type Culture Collection and cultured following the provided instructions. The murine ovarian cancer cell line ID8 (catalog no. SCC145) was sourced from Sigma-Aldrich. The human ovarian cancer cell line OVCAR8 was obtained from the Characterized Cell Line Core of MD Anderson Cancer Center. Cell lines SKOV3-Luci, OVCAR3-Luci, OVCAR8-Luci, and ID8-Luci were established through lentivirus transduction with firefly luciferase of parental cell lines, respectively. The generation of $Trp53^{-/-}$ $Brca1^{-/-}$ ID8 cell line was performed as previously described (*14*). Regular testing for mycoplasma contamination was conducted every 6 months.

Primary human T cells

Primary human T cells were isolated from healthy donors or patients with ovarian cancer at the Tongji Hospital. The protocol was approved by the institutional review board of Tongji Hospital, Tongji Medical College, Huazhong University of Science and Technology (S122-5), and informed consent was obtained from all participants. Human T cells were isolated from PBMCs using the EasySep human T cell isolation kit (STEMCELL Technologies, no. 17951) and activated with the human CD3/CD28/CD2 T cell activator following the manufacturer's instructions. T cells were cultured in OpTmizer T cell expansion medium supplemented with 5% fetal bovine serum (FBS), IL-2 (200 U/ml), IL-7 (40 ng/ml), and IL-15 (50 ng/ml). T cells with germline *BRCA2* mutations have c.9203_9210del, c.6513_6514del, or c.4363G > T on the *BRCA2* gene. Mutations were heterozygous and tested in PBMCs as previously indicated (*14*). In general, genomic DNA was extracted using the DNeasy Blood and Tissue Kit for blood samples. The purified DNA was quantified on a Qubit 4.0 (Life Technologies) to confirm a sufficient amount for downstream experiments. The extracted DNA from blood samples was captured using the Precision human HRD assay [Precision Scientific (Beijing) Co. Ltd.], which is a customized panel of probes against sites of nucleotide polymorphisms to quantify genomic regions of 36 DNA damage repair genes for germline and somatic mutation calling. The captured DNA was sequenced on an Illumina NovaSeq 6000 instrument.

CAR T cell generation and adoptive transfer

CAR sequences were synthesized and cloned into the pLVX-EF1a vector (GenScript), and 293T packaging cells were transfected to generate lentivirus. T cells were enriched from PBMCs using the

human T cell enrichment isolation kit (STEMCELL, no. 17951). T cells were activated with the human CD3/CD28/CD2 T cell activator for 1 day before transduction with CAR lentivirus. T cells were cultured in OpTmizer T cell expansion medium supplemented with 5% FBS, IL-2 (200 U/ml), IL-7 (40 ng/ml), and IL-15 (50 ng/ml). Functional assays were carried out after 8 days of in vitro culture.

T/CAR-T cells were genetically modified via electroporation using a ribonucleoprotein complex consisting of Cas9/CBE3 protein bound to sgRNAs. This process was facilitated by the Lonza P3 Primary Cell 4D-Nucleofector X kit (catalog no. V4XP-3032). Freshly isolated T cells were cultured with the human CD3/CD28/CD2 T cell activator (STEMCELL, no. 10970) for 24 hours before undergoing editing. CAR-T cells were transfected by lentivirus for 24 hours before editing. Subsequently, 20 μM sgRNA (provided by GenScript Biotech Corporation) was combined at an equimolar ratio with Cas9 or CBE3 protein (sourced from IASO Biotherapeutics) and introduced into the cells via electroporation as previously described (*41*). The efficiency of gene editing was assessed through DNA sequencing and subsequent ICE/EditR analysis, along with Western blot analysis conducted 3 days postediting.

Before CAR-T cell injection in CDX and PDX models, subcutaneous tumor size was assessed every third day using a digital caliper. Mice were distributed to different experimental arms such that each arm had an equal initial tumor burden. The day after distribution, mice were administered 5×10^6 CAR-T cells with distinct *PARP1* mutations specified for each experimental group via tail-vein injection. The tumor burden was subsequently evaluated every 3 days.

CRISPR-Cas9 screening

The CRISPR-Pool KOUT Human Library was acquired from Shanghai Genechem Co. Ltd. T cells were transfected with a genome-scale CRISPR-Cas9 knockout lentivirus library comprising 123,411 sgRNAs targeting 19,050 genes (each gene targeted by six different sgRNAs) and 1864 microRNAs (each microRNA targeted by four different sgRNAs), in addition to 1000 nontargeting control sgRNAs. Approximately 200 million T cells per replicate were transduced at a multiplicity of infection below 0.3 to ensure that most T cells carried only one sgRNA, with each sgRNA represented in around 500 T cells. Two days posttransfection, Cas9 protein was introduced into the T cells via electroporation. Puromycin selection was applied for 2 days, followed by the addition of olaparib at a concentration of 50 μM for 6 days. Genomic DNA extracted from the remaining T cells underwent polymerase chain reaction (PCR) amplification of the sgRNA cassette for Illumina sequencing of sgRNA representation. Detailed protocols for PCR amplification and Illumina sequencing can be found at https://portals.broadinstitute.org/gpp/public/resources/protocols. Data analysis was conducted using MAGeCK. To identify candidate genes, the normalized sgRNA count table was inputted into MAGeCK for comparing olaparib-treated (experimental) and vehicle (control) conditions as described above. Top genes were identified on the basis of robust rank aggregation (RRA) for all sgRNAs and *P* values.

CDX and PDX models

NSG mice were sourced from GemPharmatech and bred in the Tongji Hospital's specific pathogen–free immune-core animal facility under controlled conditions: 12-hour light/dark cycles (7:00 to 19:00 light, 150 to 300 lux), with ad libitum access to irradiated standard chow (AIN-93 formula) and autoclaved water provided via sterile bottles (replenished twice weekly). Body weight was monitored twice weekly throughout the study period. In PDX models, fresh human EOC tissues were isolated into 5 mm–by–5 mm–by–5 mm pieces and subcutaneously implanted into 6-week-old female NSG mice. Upon reaching a size of 1 cm by 1 cm by 1 cm, the tumors were aseptically harvested and propagated to the subsequent generation. In the case of subcutaneously implanted samples, a small skin incision was created in the flank region, and tumor pieces were inserted between the skin and fascia before stapling the skin. For the CDX model, 5×10^6 SKOV3 cells were injected subcutaneously into NSG mice.

Transgenic mouse tumor models

C57BL/6JGpt-*Cd4*$^{em1Cin(Cre)}$ (CD4-cre) mice and C57BL/6JG-*Parp1*$^{em1cn(LsLp.s588F)}$ (Parp1$^{S588F/+}$) mice were acquired from Gempharmatech Co. Ltd. and bred to generate T cell–specific *Parp1* mutated mice (CD4-cre; Parp1$^{S588F/\ S588F}$ mice, referred to as Thy$^{\Delta Parp1\text{-}S588F}$). Control mice were cre-negative Parp1$^{S588F/S588F}$ (Thy $^{Parp1+/+}$) mice matched in age. The mice were administered an intraperitoneal injection of an ID8 cell suspension containing 5×10^6 cells in 100 μl of phosphate-buffered saline (PBS). Tumor burden was evaluated every 5 days postinjection using noninvasive bioluminescence imaging on an in vivo imaging system (Caliper Life Sciences).

$CD8^+$ T cell depletion was accomplished by intraperitoneal injection of 100 μg of CD8β monoclonal antibody in 100 μl of PBS on days −3, −1, and day 1 and subsequently twice weekly after tumor inoculation. Control mice were administered an isotype control monoclonal antibody at the equivalent dosage in PBS. Confirmation of $CD8^+$ T cell depletion was conducted by labeling $CD8^+$ T cells from spleens and PBMCs using a CD8 monoclonal antibody followed by flow cytometry analysis.

In ICI experiments, mice with tumors were treated with anti-PD1 monoclonal antibody or rat immunoglobulin Ga isotype control antibody commencing on day 7 after tumor inoculation and subsequently twice weekly. In the case of PARPi, mice were administered olaparib at a dosage of 100 mg/kg in 100 μl or vehicle (5% dextrose) daily via oral gavage.

Statistical analysis

Individual-level data for experiments where $n < 20$ are presented in data file S1. The statistical analyses were conducted using R version 3.6 and GraphPad Prism 9 software (GraphPad Software). Each experiment was replicated at least three times, as specified in the figure legends. Various statistical tests were used for group comparisons, including the unpaired Student's *t* test between two groups, one-way analysis of variance (ANOVA) for comparison among three or more groups, and paired samples Wilcoxon signed-rank test for comparison between two groups. Normality was evaluated using Shapiro-Wilk testing (for experiments in which $n < 50$) or Kolmogorov-Smirnov testing (for experiments in which $n > 50$) with $\alpha = 0.05$ to determine the use of parametric versus nonparametric analyses. The growth of primary tumors over time was evaluated using two-way ANOVA with correction for multiple comparisons. Mouse survival curves were compared using a log-rank (Mantel-Cox) test. All *P* values were considered two-sided, and statistical significance was assessed at the 0.05 level. Significance is denoted as follows: $^*P < 0.05$, $^{**}P < 0.01$, $^{***}P < 0.001$, and $^{****}P < 0.0001$.

Supplementary Materials

The PDF file includes:
Materials and Methods
Figs. S1 to S8
Tables S1 to S5

Other Supplementary Material for this manuscript includes the following:
Data files S1 and S2
MDAR Reproducibility Checklist

REFERENCES AND NOTES

1. C. J. Lord, A. Ashworth, PARP inhibitors: Synthetic lethality in the clinic. *Science* **355**, 1152–1158 (2017).
2. N. J. Curtin, C. Szabo, Poly(ADP-ribose) polymerase inhibition: Past, present and future. *Nat. Rev. Drug Discov.* **19**, 711–736 (2020).
3. S. Lheureux, M. Braunstein, A. M. Oza, Epithelial ovarian cancer: Evolution of management in the era of precision medicine. *CA Cancer J. Clin.* **69**, 280–304 (2019).
4. P. M. Webb, S. J. Jordan, Global epidemiology of epithelial ovarian cancer. *Nat. Rev. Clin. Oncol.* **21**, 389–400 (2024).
5. P. DiSilvestro, S. Banerjee, N. Colombo, G. Scambia, B. G. Kim, A. Oaknin, M. Friedlander, A. Lisyanskaya, A. Floquet, A. Leary, G. S. Sonke, C. Gourley, A. Oza, A. González-Martín, C. Aghajanian, W. Bradley, C. Mathews, J. Liu, J. McNamara, E. S. Lowe, M. L. Ah-See, K. N. Moore, on behalf of the SOLO1 Investigators, Overall survival with maintenance olaparib at a 7-year follow-up in patients with newly diagnosed advanced ovarian cancer and a BRCA mutation: The SOLO1/GOG 3004 trial. *J. Clin. Oncol.* **41**, 609–617 (2023).
6. A. González-Martín, B. Pothuri, I. Vergote, R. DePont Christensen, W. Graybill, M. R. Mirza, C. McCormick, D. Lorusso, P. Hoskins, G. Freyer, K. Baumann, K. Jardon, A. Redondo, R. G. Moore, C. Vulsteke, R. E. O'Cearbhaill, B. Lund, F. Backes, P. Barretina-Ginesta, A. F. Haggerty, M. J. Rubio-Pérez, M. S. Shahin, G. Mangili, W. H. Bradley, I. Bruchim, K. Sun, I. A. Malinowska, Y. Li, D. Gupta, B. J. Monk, Niraparib in patients with newly diagnosed advanced ovarian cancer. *N. Engl. J. Med.* **381**, 2391–2402 (2019).
7. J. S. Frenel, J. W. Kim, N. Aryal, R. Asher, D. Berton, L. Vidal, P. Pautier, J. A. Ledermann, R. T. Penson, A. M. Oza, J. Korach, T. Huzarski, S. Pignata, N. Colombo, T. W. Park-Simon, K. Tamura, G. S. Sonke, A. E. Freimund, C. K. Lee, E. Pujade-Lauraine, Efficacy of subsequent chemotherapy for patients with BRCA1/2-mutated recurrent epithelial ovarian cancer progressing on olaparib versus placebo maintenance: Post-hoc analyses of the SOLO2/ENGOT Ov-21 trial. *Ann. Oncol.* **33**, 1021–1028 (2022).
8. U. A. Matulonis, L. Walder, T. J. Nøttrup, P. Bessette, S. Mahner, M. Gil-Martin, E. Kalbacher, J. A. Ledermann, R. M. Wenham, K. Woie, S. Lau, F. Marmé, A. Casado Herraez, A. C. Hardy-Bessard, S. Banerjee, G. Lindahl, B. Benigno, J. Buscema, K. Travers, H. Guy, M. R. Mirza, Niraparib maintenance treatment improves time without symptoms or toxicity (TWiST) versus routine surveillance in recurrent ovarian cancer: A TWiST analysis of the ENGOT-OV16/NOVA trial. *J. Clin. Oncol.* **37**, 3183–3191 (2019).
9. M. P. Dias, S. C. Moser, S. Ganesan, J. Jonkers, Understanding and overcoming resistance to PARP inhibitors in cancer therapy. *Nat. Rev. Clin. Oncol.* **18**, 773–791 (2021).
10. J. L. Oliveira, P. T. Greipp, A. Rangan, A. Jatoi, P. L. Nguyen, Myeloid malignancies in cancer patients treated with poly(ADP-ribose) polymerase (PARP) inhibitors: A case series. *Blood Cancer J.* **12**, 11 (2022).
11. P. Chiusolo, C. Marchetti, M. Rossi, G. Minnella, V. Salutari, M. Distefano, S. Giammarco, E. Metafuni, A. Minucci, F. Frioni, C. Gasbarrino, M. Colangelo, D. Orteschi, A. Fagotti, D. Lorusso, L. Pagano, V. De Stefano, G. Scambia, S. Sica, A common pattern of somatic mutations in t-MDS/AML of patients treated with PARP inhibitors for metastatic ovarian cancer. *Am. J. Hematol.* **97**, E400–e403 (2022).
12. C. Pantelidou, O. Sonzogni, M. De Oliveria Taveira, A. K. Mehta, A. Kothari, D. Wang, T. Visal, M. K. Li, J. Pinto, J. A. Castrillon, E. M. Cheney, P. Bouwman, J. Jonkers, S. Rottenberg, J. L. Guerriero, G. M. Wulf, G. I. Shapiro, PARP inhibitor efficacy depends on $CD8^+$ T-cell recruitment via intratumoral STING pathway activation in BRCA-deficient models of triple-negative breast cancer. *Cancer Discov.* **9**, 722–737 (2019).
13. A. V. R. Kornepati, C. M. Rogers, P. Sung, T. J. Curiel, The complementarity of DDR, nucleic acids and anti-tumour immunity. *Nature* **619**, 475–486 (2023).
14. Y. Luo, Y. Xia, D. Liu, X. Li, H. Li, J. Liu, D. Zhou, Y. Dong, X. Li, Y. Qian, C. Xu, K. Tao, G. Li, W. Pan, Q. Zhong, X. Liu, S. Xu, Z. Wang, R. Liu, W. Zhang, W. Shan, T. Fang, S. Wang, Z. Peng, P. Jin, N. Jin, S. Shi, Y. Chen, M. Wang, X. Jiao, M. Luo, W. Gong, Y. Wang, Y. Yao, Y. Zhao, X. Huang, X. Ji, Z. He, G. Zhao, R. Liu, M. Wu, G. Chen, L. Hong, D. Ma, Y. Fang, H. Liang, Q. Gao, Neoadjuvant PARPi or chemotherapy in ovarian cancer informs targeting effector Treg cells for homologous-recombination-deficient tumors. *Cell* **187**, 4905–4925.e24 (2024).
15. J. Shen, W. Zhao, Z. Ju, L. Wang, Y. Peng, M. Labrie, T. A. Yap, G. B. Mills, G. Peng, PARPi triggers the STING-dependent immune response and enhances the therapeutic efficacy of immune checkpoint blockade independent of BRCAness. *Cancer Res.* **79**, 311–319 (2019).
16. M. A. Ghonim, S. V. Ibba, A. F. Tarhuni, Y. Errami, H. H. Luu, M. J. Dean, A. H. El-Bahrawy, D. Wyczechowska, I. A. Benslimane, L. Del Valle, A. A. Al-Khami, A. C. Ochoa, A. H. Boulares, Targeting PARP-1 with metronomic therapy modulates MDSC suppressive function and enhances anti-PD-1 immunotherapy in colon cancer. *J. Immunother. Cancer* **9**, e001643 (2021).
17. J. Park, J. C. Kim, M. Lee, J. Lee, Y. N. Kim, Y. J. Lee, S. Kim, S. W. Kim, S. H. Park, J. Y. Lee, Frequency of peripheral $PD\text{-}1^+$ regulatory T cells is associated with treatment responses to PARP inhibitor maintenance in patients with epithelial ovarian cancer. *Br. J. Cancer* **129**, 1841–1851 (2023).
18. E. Ghisoni, M. Morotti, A. Sarivalasis, A. J. Grimm, L. Kandalaft, D. D. Laniti, G. Coukos, Immunotherapy for ovarian cancer: Towards a tailored immunophenotype-based approach. *Nat. Rev. Clin. Oncol.* **21**, 801–817 (2024).
19. A. Ribas, J. D. Wolchok, Cancer immunotherapy using checkpoint blockade. *Science* **359**, 1350–1355 (2018).
20. T. A. Yap, A. Bardia, M. Dvorkin, M. D. Galsky, J. T. Beck, D. R. Wise, O. Karyakin, G. Rubovszky, N. Kislov, K. Rohrberg, A. A. Joy, M. L. Telli, A. M. Schram, U. Conte, C. Chappey, R. Stewart, D. Stypinski, E. Michelon, R. Cesari, P. A. Konstantinopoulos, Avelumab plus talazoparib in patients with advanced solid tumors: The JAVELIN PARP medley nonrandomized controlled trial. *JAMA Oncol.* **9**, 40–50 (2023).
21. V. Makker, C. Aghajanian, A. L. Cohn, M. Romeo, R. Bratos, M. S. Brose, M. Messing, L. Dutta, C. E. Dutcus, J. Huang, E. V. Schmidt, R. Orlowski, M. H. Taylo, A phase Ib/II study of lenvatinib and pembrolizumab in advanced endometrial carcinoma (study 111/KEYNOTE-146): Long-term efficacy and safety update. *J. Clin. Oncol.* **41**, 974–979 (2023).
22. K. Fizazi, M. Retz, D. P. Petrylak, J. C. Goh, J. Perez-Gracia, L. Lacombe, S. Zschäbitz, M. Burotto, H. Mahammedi, G. Gravis, D. A. Bastos, S. L. McCune, J. C. Vázquez Limón, E. M. Kwan, D. Castellano, A. Fléchon, F. Saad, M. O. Grimm, D. R. Shaffer, A. J. Armstrong, P. Bhagavatheeswaran, N. P. Amin, K. Ünsal-Kaçmaz, X. Wang, J. Li, A. Loehr, R. K. Pachynski, Nivolumab plus rucaparib for metastatic castration-resistant prostate cancer: Results from the phase 2 CheckMate 9KD trial. *J. Immunother. Cancer* **10**, e004761 (2022).
23. U. A. Matulonis, R. Shapira-Frommer, A. D. Santin, A. S. Lisyanskaya, S. Pignata, I. Vergote, F. Raspagliesi, G. S. Sonke, M. Birrer, D. M. Provencher, J. Sehouli, N. Colombo, A. González-Martín, A. Oaknin, P. B. Ottevanger, V. Rudaitis, K. Katchar, H. Wu, S. Keefe, J. Ruman, J. A. Ledermann, Antitumor activity and safety of pembrolizumab in patients with advanced recurrent ovarian cancer: Results from the phase II KEYNOTE-100 study. *Ann. Oncol.* **30**, 1080–1087 (2019).
24. J. Liu, X. Jiao, D. Ma, Y. Fang, Q. Gao, CAR-T therapy and targeted treatments: Emerging combination strategies in solid tumors. *Med* **5**, 530–549 (2024).
25. Y. Zeng, O. Arisa, C. J. Peer, W. D. Figg, A. Fojo, PARP inhibitors: A review of the pharmacology, pharmacokinetics, and pharmacogenetics. *Semin. Oncol.* **51**, 19–24 (2023).
26. J. Joung, S. Konermann, J. S. Gootenberg, O. O. Abudayyeh, R. J. Platt, M. D. Brigham, N. E. Sanjana, F. Zhang, Genome-scale CRISPR-Cas9 knockout and transcriptional activation screening. *Nat. Protoc.* **12**, 828–863 (2017).
27. B. Wang, M. Wang, W. Zhang, T. Xiao, C. H. Chen, A. Wu, F. Wu, N. Traugh, X. Wang, Z. Li, S. Mei, Y. Cui, S. Shi, J. J. Lipp, M. Hinterndorfer, J. Zuber, M. Brown, W. Li, X. S. Liu, Integrative analysis of pooled CRISPR genetic screens using MAGeCKFlute. *Nat. Protoc.* **14**, 756–780 (2019).
28. M. F. Langelier, J. L. Planck, S. Roy, J. M. Pascal, Structural basis for DNA damage-dependent poly(ADP-ribosyl)ation by human PARP-1. *Science* **336**, 728–732 (2012).
29. S. J. Pettitt, D. B. Krastev, I. Brandsma, A. Dréan, F. Song, R. Aleksandrov, M. I. Harrell, M. Menon, R. Brough, J. Campbell, J. Frankum, M. Ranes, H. N. Pemberton, R. Rafiq, K. Fenwick, A. Swain, S. Guettler, J. M. Lee, E. M. Swisher, S. Stoynov, K. Yusa, A. Ashworth, C. J. Lord, Genome-wide and high-density CRISPR-Cas9 screens identify point mutations in PARP1 causing PARP inhibitor resistance. *Nat. Commun.* **9**, 1849 (2018).
30. A. Schambach, C. J. Buchholz, R. Torres-Ruiz, K. Cichutek, M. Morgan, I. Trapani, H. Büning, A new age of precision gene therapy. *Lancet* **403**, 568–582 (2023).
31. M. G. Kluesner, D. A. Nedveck, W. S. Lahr, J. R. Garbe, J. E. Abrahante, B. R. Webber, B. S. Moriarity, EditR: A method to quantify base editing from sanger sequencing. *CRISPR J.* **1**, 239–250 (2018).
32. E. Schoutrop, I. El-Serafi, T. Poiret, Y. Zhao, O. Gultekin, R. He, L. Moyano-Galceran, J. W. Carlson, K. Lehti, M. Hassan, I. Magalhaes, J. Mattsson, Mesothelin-specific CAR T cells target ovarian cancer. *Cancer Res.* **81**, 3022–3035 (2021).
33. S. L. Maude, T. W. Laetsch, J. Buechner, S. Rives, M. Boyer, H. Bittencourt, P. Bader, M. R. Verneris, H. E. Stefanski, G. D. Myers, M. Qayed, B. De Moerloose, H. Hiramatsu, K. Schlis, K. L. Davis, P. L. Martin, E. R. Nemecek, G. A. Yanik, C. Peters, A. Baruchel, N. Boissel, F. Mechinaud, A. Balduzzi, J. Krueger, C. H. June, B. L. Levine, P. Wood, T. Taran, M. Leung, K. T. Mueller, Y. Zhang, K. Sen, D. Lebwohl, M. A. Pulsipher, S. A. Grupp, Tisagenlecleucel in children and young adults with B-cell lymphoblastic leukemia. *N. Engl. J. Med.* **378**, 439–448 (2018).
34. B. D. Shah, A. Ghobadi, O. O. Oluwole, A. C. Logan, N. Boissel, R. D. Cassaday, T. Leguay, M. R. Bishop, M. S. Topp, D. Tzachanis, K. M. O'Dwyer, M. L. Arellano, Y. Lin, M. R. Baer,

G. J. Schiller, J. H. Park, M. Subklewe, M. Abedi, M. C. Minnema, W. G. Wierda, D. J. DeAngelo, P. Stiff, D. Jeyakumar, C. Feng, J. Dong, T. Shen, F. Milletti, J. M. Rossi, R. Vezan, B. K. Masouleh, R. Houot, KTE-X19 for relapsed or refractory adult B-cell acute lymphoblastic leukaemia: Phase 2 results of the single-arm, open-label, multicentre ZUMA-3 study. *Lancet* **398**, 491–502 (2021).
35. S. E. Lindner, S. M. Johnson, C. E. Brown, L. D. Wang, Chimeric antigen receptor signaling: Functional consequences and design implications. *Sci. Adv.* **6**, eaaz3223 (2020).
36. E. K. Lee, P. A. Konstantinopoulos, Combined PARP and immune checkpoint inhibition in ovarian cancer. *Trends Cancer* **5**, 524–528 (2019).
37. D. Menolfi, B. J. Lee, H. Zhang, W. Jiang, N. E. Bowen, Y. Wang, J. Zhao, A. Holmes, S. Gershik, R. Rabadan, B. Kim, S. Zha, ATR kinase supports normal proliferation in the early S phase by preventing replication resource exhaustion. *Nat Commun.* **14**, 3618 (2023).
38. L. Moreno-Lama, M. A. Galindo-Campos, C. Martínez, L. Comerma, I. Vazquez, M. Vernet-Tomas, C. Ampurdanés, N. Lutfi, J. Martin-Caballero, F. Dantzer, M. Quintela-Fandino, S. O. Ali, J. Jimeno, J. Yélamos, Coordinated signals from PARP-1 and PARP-2 are required to establish a proper T cell immune response to breast tumors in mice. *Oncogene* **39**, 2835–2843 (2020).
39. N. Lutfi, C. Martínez, J. Yélamos, Studying the immunomodulatory functions of PARP1 and PARP2 in mouse models of cancer. *Methods Mol. Biol.* **2609**, 195–212 (2023).
40. A. K. Mehta, E. M. Cheney, C. A. Hartl, C. Pantelidou, M. Oliwa, J. A. Castrillon, J. R. Lin, K. E. Hurst, M. de Oliveira Taveira, N. T. Johnson, W. M. Oldham, M. Kalocsay, M. J. Berberich, S. A. Boswell, A. Kothari, S. Johnson, D. A. Dillon, M. Lipschitz, S. Rodig, S. Santagata, J. E. Garber, N. Tung, J. Yélamos, J. E. Thaxton, E. A. Mittendorf, P. K. Sorger, G. I. Shapiro, J. L. Guerriero, Targeting immunosuppressive macrophages overcomes PARP inhibitor resistance in BRCA1-associated triple-negative breast cancer. *Nat. Cancer* **2**, 66–82 (2021).
41. Y. Cheng, J. Zhang, W. Mu, S. Ye, J. Cheng, L. Zhu, G. Wang, Y. Cao, D. Li, G. Hu, L. Huang, J. Wang, J. Zhou, Dasatinib-resistant universal CAR-T cells proliferate in the presence of host immune cells and exhibit antitumor activity. *Mol. Ther.* **33**, 1535–1551 (2025).

Acknowledgments: We would like to thank all patients and providers who participated in this study. We would like to express our gratitude to J. Yélamos and his team for contributions to exploring the roles of PARP1 and PARP2 in T cells, which have enlightened our understanding throughout this study. **Funding:** This work was supported by National Key Technology Research and Development Program of China 2022YFC2704200 and 2022YFC2704205 (to Q.G. and Y.F.), National Science Foundation of China 82272707 (to Y.F.), National Science Foundation of China 82441045 (to Y.F.), National Science Foundation of China 81772787 (to Q.G.), National Science Foundation of China 82072889 (to Q.G.), Beijing Xisike Clinical Oncology research foundation (to X.J. and Q.G.), Innovation Group Project of Hubei Province 2023AFA036 (to Y.F.), Breast Cancer Research Foundation (to G.B.M.), and the Sheldon and Miriam Adelson Medical Research Foundation (to G.B.M.). **Author contributions:** J.L., Q.G., and Y.F. conceived and designed the study. J.L., X.J., and W.M. developed the methodology. J.L., X.J., W.M., H.L., Y.X., Y.W., L.Z., Q.Z., W.P., X.L., M.X., J.C., H.L., X.Z., Z.D., and G.H. conducted the investigation and performed experiments. J.L., X.J., and W.M. were responsible for data visualization. G.B.M., Q.G., and Y.F. acquired funding to support the research. J.L., Q.G., and Y.F. administered the project. G.B.M., D.M., Q.G., and Y.F. provided supervision throughout the study. J.L., X.J., and W.M. wrote the original draft of the manuscript. All authors, including J.L., X.J., W.M., G.B.M., D.M., Q.G., and Y.F., participated in reviewing and editing the manuscript. **Competing interests:** G.B.M. serves as a scientific advisory board member or consultant for multiple organizations, including Astex, Ellipses Pharmaceuticals, ImmunoMET, Ionis, Leapfrog Bio, Bruker/Nanostring, Neophore, Nerviano, Nuvectis, Pangea, PDX Pharmaceuticals, Qureator, Rybodyne, Signalchem Lifesciences, Tarveda, Turbine, and Zentalis Pharmaceuticals. G.B.M. holds stock, options, or other financial interests in several companies: Bluedot, Catena Pharmaceuticals, ImmunoMet, Nuvectis, RyboDyne, SignalChem Lifesciences, Tarveda, and Turbine. In addition. G.B.M. has licensed technology to Myriad Genetics (HRD assay) and Nanostring (DSP technology). G.B.M.'s research has received foundation support from the Adelson Medical Research Foundation, Breast Cancer Research Foundation, Komen Research Foundation, Ovarian Cancer Research Foundation, and Prospect Creek Foundation. Sponsored research support has been provided by AstraZeneca, Zentalis, Nanostring, and Ionis (through provision of tool compounds). G.B.M. has also received clinical trials support (either funding or in-kind contributions) from AstraZeneca, Genentech, GSK, and Lilly. G.H. is employed by Nanjing IASO Biotherapeutics Ltd. Z.D. is employed by Fynn Biotechnologies. The other authors declare that they have no competing interests. **Data and materials availability:** All data associated with this study are present in the paper or the Supplementary Materials. Processed, deidentified scRNA-seq data analyzed in this study are publicly available at the Gene Expression Omnibus (GEO) under the accession number GSE222557 (*14*). Raw data for all experiments where $n < 20$ are listed in data file S1. Images of unedited blots are included in data file S2.

Submitted 1 October 2024
Accepted 12 March 2025
Published 7 May 2025
10.1126/scitranslmed.adr5861